Eidgenössische Technische Hochschule Zürich
Swiss Federal Institute of Technology Zurich

RRE
Reliability & Risk Engineering

Empa
Materials Science and Technology

Roxanne Vandenberghe

Optimal sizing and operation of a hydrogen generation site considering waste heat recovery

Master Thesis

RRE – Reliability and Risk Engineering Lab
Swiss Federal Institute of Technology (ETH) Zürich
Empa – Swiss Federal Laboratories for Materials Science and Technology

Expert
Prof. Dr. Giovanni Sansavini
Supervisors
Dr. Gabriele Humbert
Dr. Hanmin Cai
Dr. Binod Prasad Koirala

Zürich, December 22, 2023

Abstract

As society strives towards net-zero emissions, hydrogen is emerging as a promising transport fuel and energy carrier. However, enhancing the competitiveness of hydrogen production via electrolysis, in comparison to natural gas reforming and coal gasification, remains a challenge.

To address this, the thesis proposes a mixed integer linear program designed to optimize the size and operation of a hydrogen generation site's components for minimal cost. The model investigates the recovery of heat generated during electrolyser operation as a strategy to lower the levelized cost of hydrogen. Furthermore, it incorporates accurate representations of the component cost and operation curves, with a special emphasis on the electrolyser. Lastly, a comprehensive sensitivity analysis, including a global sensitivity analysis and an examination of individual parameters' influence, is conducted on the model outcome.

The results suggest that the strategy of recovering and exporting waste heat to a high-temperature district heating network can effectively reduce the cost of hydrogen production from electrolysis. When combined with the simultaneous optimization of the sizing and operation of the site components, a decrease in the value-adjusted levelized cost of hydrogen (VALCOH) of 18.9% is achieved. An accurate representation of electrolyser efficiency influences both the size of the chosen plant equipment, as well as the usage of partial load during electrolyser operation. By increasing the number of break points of a piecewise affine approximation of the efficiency curve from 1 to 4, the VALCOH decreases by 3.9%. The sensitivity analysis ultimately highlights the substantial influence of the electricity price and electrolyser efficiency.

In conclusion, this work shows the relevance of incorporating waste heat recovery to reduce costs of a hydrogen generation site. It also emphasizes the importance of simultaneous optimization for the size and operation of components in multi-energy systems. Furthermore, it underscores that an accurate representation of the electrolyser efficiency has a profound impact on the VALCOH.

Acknowledgements

I would like to express my deepest gratitude to my supervisors, Gabriele Humbert, Hanmin Cai, and Binod Prasad Koirala. Their extensive knowledge and unwavering guidance have been instrumental in the completion of this thesis. I am also grateful to professor Giovanni Sansavini for his oversight of this thesis. His knowledge and commitment to the highest standards inspired and motivated me.

My sincere thanks also go to my colleagues and the PhD students at the RRE lab. The stimulating discussions, the shared lunches, and the much-needed coffee breaks were very much appreciated. Their friendship made this journey a pleasant one.

I would also like to thank my sister, who was always available for a call when I needed to vent or seek advice. To my friends, thank you for the pep talks, the laughter, and the great moments we shared. Lastly, I would like to acknowledge my family, whose belief in my abilities has always been a source of encouragement for me.

In conclusion, I recognize that this research would not have been possible without the support and assistance of many people and I am extremely thankful for their inspiration and encouragement.

Contents

List of Acronyms

COP	Coefficient of Performance
DHN	District Heating Network
EE	Elementary Effect
GSA	Global Sensitivity Analysis
HEX	Heat exchanger
HHV	Higher Heating Value
HP	Heat Pump
HT	High-Temperature
H_2	Hydrogen
LCOH	Levelized Cost of Hydrogen
MILP	Mixed Integer Linear Program
MT	Medium-Temperature
NOCT	Nominal Operating Cell Temperature
PEM	Proton Exchange Membrane
PV	Photovoltaic
PWA	Piecewise Affine
RES	Renewable Energy Source
SOC	State Of Charge
UP	Unit Price
VALCOH	Value-Adjusted Levelized Cost of Hydrogen

List of Symbols

a	annuity factor (-)
C	cost (kEUR)
c	specific heat capacity (kJ/(kg K))
d	discount rate (-)
E	energy (kWh)
f	model output/objective function (kEUR/y)
G	irradiance (kW/m^2)
i	PWA section index
j	PWA section index
K	capacity (kWh)
k	number of sample points
l	number of sections in PWA approximation
m	mass (kg)
$\dot{m}$	mass flow (kg/s)
n	number of breakpoints of PWA approximation
P	power (kW)
p	GSA input parameter index
Q	heat power (kW)
q	number of input parameters considered in the GSA
r	sample point index
S	size (kW // m^2)
s	equipment size corresponding to breakpoints (kW)
T	temperature (°C)
t	timestep (-)
u	model input parameter considered in the GSA
x	binary variable for on/off status (-)
y	binary variable for PWA section (-)

Greek letters

α	cost coefficient (kEUR/kW)
β	cost coefficient (kEUR)
γ	solar radiation dependence PV cell efficiency (-)
Δ	time variation (h)
δ	increment
ε	efficiency coefficient (-)
ζ	temperature dependence PV cell efficiency (K)
η	efficiency (-)
μ	mean value
ν	fixed penalty (EUR)
ξ	maintenance cost fraction (-)
π	cost of an energy carrier (EUR/kWh)
σ	standard deviation
ϕ	heat recovery fraction (-)
ω	efficiency coefficient (-)

Subscripts

a	ambient
ann	annual
b	battery
c	compressor
ch	charge
cw	cooling water
disch	discharge
disp	dispenser
e	electrolyser
el	electricity
emp	empirical
exp	exported
imp	imported
in	inlet
inv	investment
lm	logarithmic
maint	maintenance
max	maximum
min	minimum
obj	objective
op	operational
out	outlet
p	at constant pressure
prod	produced
rec	recovered
ref	reference
ret	return
refr	refrigerator
start	startup
stor	storage
sup	supply
t	at timestep t
th	thermal
tot	total

List of Figures

List of Tables

Chapter 1

Introduction

The escalating threat of climate change, driven by a rise in global temperatures and the overuse of our carbon budget, presents an urgent challenge that requires imminent action. To limit global warming to 1.5°C, significant efforts across all economic sectors are required to reduce carbon dioxide emissions. The transition to low-carbon and even net-zero energy systems is crucial to achieve the goals set in international climate agreements [5]. Renewable energy sources such as wind power and solar photovoltaics (PV) can provide low-carbon electricity, but also have their drawbacks. They are intermittent sources of energy that are non-dispatchable and therefore complicate the matching of supply and demand within the energy system. Thus, the production of hydrogen via electrolysis, the splitting of water into hydrogen and oxygen using electricity, is a great measure in allowing flexibility in the generation. Additionally, hydrogen has been identified as a valuable energy carrier, an attractive option for sectors with emissions that are hard to abate, such as transportation and heavy industry [6, 7].

Nonetheless, clean hydrogen production is facing a multitude of challenges. Firstly, natural gas reforming and coal gasification account for over 95% of the world's hydrogen production today and the use of these energy sources has a significant impact on the CO_2 emissions attributed to the production of hydrogen [8]. Therefore, hydrogen is far from a clean energy source if carbon capture and storage is not implemented. Secondly, due to high cost associated with water electrolysis and renewables, less than 0.1% of the global hydrogen production comes from a combination of water electrolysis and low-carbon energy. Thus, developments are necessary in the field of water electrolysers in order to, on the one hand, increase efficiency of the electrolysis; and on the other hand, to find a purposeful application for the electrolyser by-products.

On another note, energy systems integration is identified as the key to decarbonising the European economy by the European Commission and is defined as follows: "the coordinated planning and operation of the energy system 'as a whole', across multiple energy carriers, infrastructures, and consumption sectors" [9]. Policy makers are thus stressing the importance of multi-energy systems and sector coupling and research in

this field is increasing [10, 11].

Therefore, the goal of this thesis is to model the optimal sizing and operation of a PV-battery coupled hydrogen generation site, taking into account waste heat recovery from the electrolyzer to supply heat to a district heating network (DHN). A literature review is conducted to frame the topic within the current standing of research. This review looks into different aspects of this topic: the optimal sizing and operation of hydrogen generation sites, detailed electrolyser operation and waste heat recovery from electrolysers. The objective of the review is to get a clear view on the progress that has been made so far in modelling hydrogen facilities, as well as identifying areas in which improvement is key to achieve more detailed and reliable results for the simulation. This master thesis then addresses part of the existing knowledge gaps identified in the next section.

1.1 Literature Review

According to the IEA, the demand for hydrogen has more than tripled since 1975, and its production contributed to 830 million tonnes of CO_2 emissions in 2018 [8]. On the one hand, hydrogen production methods such as steam methane reforming and coal gasification, while well-established and inexpensive, are CO_2 intensive. These methods produce hydrogen at costs ranging between 2 to 6 and 2 to 3 dollars per kg, respectively [12]. On the other hand, green hydrogen can be produced through autothermal reforming of green ammonia, biogas cracking and water electrolysis, with the latter being the most established [13]. To qualify as green hydrogen, the electrolyser must be powered by electricity from renewable sources. However, the cost of hydrogen produced via water electrolysis ranges from 5.6 to 15.7 EUR/kg, therefore making it economically less attractive than fossil fuel-based hydrogen. Despite this, electrolysers present a compelling technical solution for transitioning to a fossil fuel-independent society.

Electrolysers generate hydrogen and oxygen from water by applying an electrical current over an electrolyser cell. The chemical reaction that occurs is the following:

$$H_2O_{(l)} \rightarrow H_{2(g)} + \frac{1}{2}O_{2(g)} \tag{1.1}$$

The three main types of electrolysers that are being researched are alkaline electrolysers, proton exchange membrane (PEM) electrolysers and solid oxide electrolysers. At present only the first two are widely commercially available [12]. Despite being the most mature technology, alkaline electrolysers have several drawbacks compared to PEM electrolysers, such as a low current density and lower flexibility in terms of system load [14]. PEM electrolysers have a larger current density and perform better under dynamic load, making them more suitable for coupling with intermittent green energy sources. However, they are significantly more expensive than alkaline electrolysers [15].

The integration of hydrogen production with renewable electricity sources in multi-energy systems is increasingly studied in literature. For instance, Minutillo et al. mod-

elled a hydrogen refuelling station with both a grid connection and a PV installation [2]. The generation objective varied between 50, 100 and 200 kg/day, and the size of the PV plant was also variable. The configurations resulted in a levelized cost of hydrogen (LCOH) ranging from 9.29 to 12.48 EUR/kg. Both the plant size and the share of electricity supplied by the grid and PV plant notably influenced the LCOH. However, this study only optimized plant operation, with component sizes being fixed. In contrast, a study by Rioja et al. carried out the simultaneous optimization of component size and system control using a Particle Swarm Optimization algorithm [16]. The largest impact on the system competitiveness was attributed to the electrolyser cost, presenting the highest potential to decrease the LCOH. Furthermore, [17] presented a method to perform the simultaneous optimization for a hydrogen plant supplied with wind power. This study looked at the different wind turbine configurations in great detail and implemented the problem as a mixed integer linear program (MILP). They found values for the LCOH varying from 2.02 EUR/kg for a non-dedicated system, all the way to 17.2 EUR/kg for a dedicated offshore wind farm.

In optimization problems that aim to minimize the costs of electrolyser operation, [18] emphasizes the importance of detailed modelling of the electrolyser. The study also calls for further research where investment decisions are made and additional revenue streams from the electrolyser are considered. In this context, [19] presents a detailed model for PEM electrolysers, formulated as a MILP. This model is subsequently used in [1], where the electrolyser efficiency is approximated by n line segments connecting $n + 1$ breakpoints on the curve, referred to as a piecewise affine (PWA) approximation. The paper introduces a novel MILP methodology that reduces the complexity of the optimal design and operation of a multi-energy system optimization problem by coupling typical design days. Moreover, [20] optimized the optimal size and hourly dispatch of components for an insular community, taking into account component degradation as well as seasonal storage. Considering the community's dependence on intermittent renewable electricity sources, they implemented PWA approximations of the electrolyser and fuel cell efficiencies to optimize the energy system. Metaheuristic techniques were shown to perform worse than a MILP formulation of the problem, albeit being less computationally intensive.

The above mentioned papers do not consider the recovery of waste heat from the electrolyser, as developed in [14] and [12]. In these theses, models are developed to estimate the heat recovery from PEM and alkaline electrolysers, using a detailed electrochemical, thermal and cooling model. The model worked out in [14] results in a thermal efficiency of 92% of the waste heat recovery system, with a cooling water temperature at less than 3°C below stack operating temperature. Furthermore, [12] found an increase of the overall system efficiency from 76.7% to 94.7% when taking into account waste heat recovery for a PEM electrolyser. Heat was found to have applications in a district heating network and could be sold to it at a competitive price. This topic is further explored by van der Roest et al., where both local coupling and DHN exports were considered [21]. An increase of the electrolyser system efficiency from 76% to 90% was calculated and it was

determined that realizing a business case is more difficult when a heat pump (HP) has to be used to increase the temperature of the heat. The distance to the end consumer was also shown to have a large influence on the levelized cost of heat, with economically feasible distances varying between one and three kilometers.

Almost all the papers cited above have implemented a sensitivity analysis in one way or another, but apart from varying the cost of certain components, not much has been done. Therefore, implementing a more rigorous global sensitivity analysis that looks at more parameters than merely the cost, is an interesting path to explore. This could identify parameters that were not considered before and thus lead to interesting insights in the developed models.

1.2 Research questions

Based on the literature review, it is apparent that there is a lack of research combining the fronts of simultaneous optimization of multi-energy system component sizes and operation, waste heat recovery from electrolysers and detailed operational models of energy system components. Thus, the research questions investigated in this thesis are the following:

1. What is the optimal size and operation of components in a hydrogen generation site with waste heat recovery in order to minimize total cost?
2. How does the modelling level of fidelity affect the identified optimal solution?
3. What heat recovery system should be implemented?
4. What inputs have the largest effect on the optimal solution and what is their effect?

1.3 Thesis contributions and organization

To summarize, the contributions of this work are threefold:

1. MILP that simultaneously optimizes the multi-energy system component size and operation to minimize the total annual cost of the site, taking into account accurate representations of the component cost and operation curves (especially the electrolyser).
2. Integration of a waste heat recovery model in the MILP and assessment of this addition to the cost of hydrogen production.
3. Twofold rigorous sensitivity analysis on the results including a global sensitivity analysis followed by an analysis of individual parameters' influence.

With these contributions, this thesis aims to be a useful tool in the design and operation of hydrogen generation sites where waste heat recovery is implemented.

The rest of the thesis is organized as follows. Chapter 2 discusses the proposed optimization model and its implementation as a MILP. Chapter 3 describes the case study to which the model is applied in terms of input data and system-specific values. Further, Chapter 4 analyzes the obtained results and performs a sensitivity analysis. Finally, Chapter 5 concludes the report and gives an outlook to future works.

Chapter 2

Methodology

This chapter introduces the methods and model used to answer the research questions. The goal of finding the optimal size and operation of a hydrogen generation site where electrolyser waste heat is recovered is reached by implementing this problem as a mixed integer linear program. First, the energy system components of the hydrogen generation site are introduced. Further, the constituents of the MILP are set forth, explaining the decision variables, required inputs, constraints and objective function. Once the model is explained fully, its novel contributions are highlighted. Lastly, the sensitivity analysis section introduces the methods that are applied to determine the parameters to which the model is most sensitive.

2.1 Energy system

The MILP developed in this thesis was based on the model developed by Humbert et al. [3], used as a reference point to which additional features have been added to answer the research questions. The baseline model covers the optimization of a PV-battery-electrolyser plant, with constant efficiency and cost for all components [3]. The hydrogen energy system developed in this report has more added complexity. Both the grid and a PV-battery system are used to power the electrolyser and the compressor, used to increase the hydrogen pressure from 30 bar to 900 bar [22]. Heat is recovered from the electrolyser by means of a cooling circuit. This cooling loop exchanges heat with a secondary cooling loop, which in turn delivers the heat to either a high-temperature (HT) district heating network ($Q_{DHN,HT}$), or to a medium-temperature (MT) district heating network ($Q_{DHN,MT}$) or a dry cooler. Heat is delivered to the high-temperature DHN by using a heat pump to upgrade the heat to the required temperature level. For the medium-temperature DHN a heat exchanger suffices. The dry cooler is taken into account to ensure continuous operation, in case the optimal plant operation includes timesteps where no heat is exported to a DHN and/or maintenance works are carried out. Any excess PV power is sold to the grid at day-ahead prices. Figure 2.1 shows a

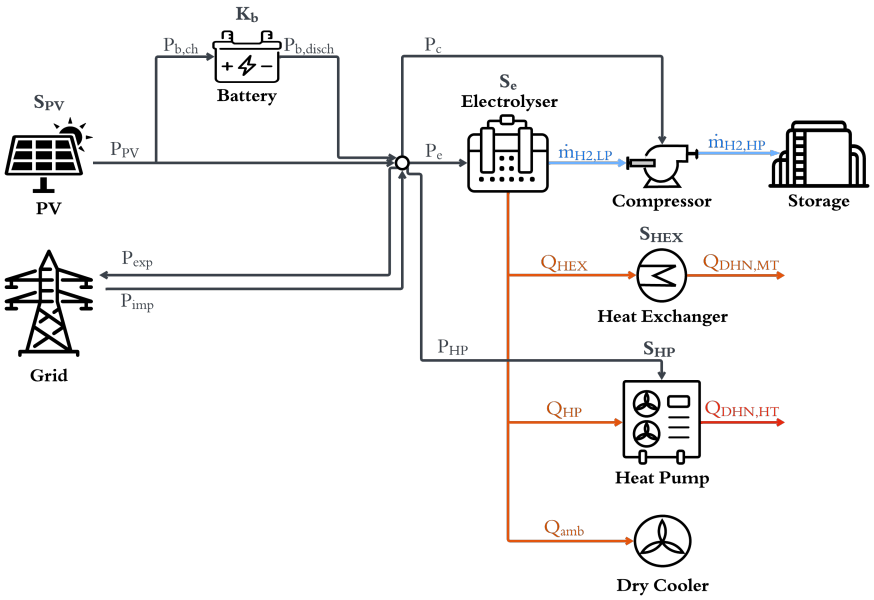

Figure 2.1: Schematic representation of the hydrogen generation site, indicating all possible components and the notation of their working power.

graphical representation of the site setup and components. The final energy system, as selected by the optimizer, can differ from the one shown in Figure 2.1, as the optimizer can decide on a zero value for the size of certain components.

2.2 Decision variables

The optimization will return the components' optimal size and operation for the horizon of one year, with hourly resolution. Thus, the time variable t will range from t_1 to t_{end}, with t_1 equalling 1 and t_{end} equalling 8760. The decision variables included the following:

1. Sizing decision variables that define the optimal size of components in the site. These are the electrolyser size (S_e), PV field area (S_{PV}), the battery capacity (K_b), as well as the heat pump size (S_{HP}) and heat exchanger area (S_{HEX}).
2. Continuous operational decision variables that correspond to the working power of each component at every timestep.
   (a) Excluding the heat recovery system, this encompasses the electrolyser input and output power (P_e and P_{H_2}), the battery charging and discharging power (P_{ch} and P_{disch}) as well as the battery energy (E_b). Further, the imported and exported grid power (P_{imp} and P_{exp}) are included here.
   (b) Specific to the heat recovery system, $\dot{m}_{cw}$ denotes the cooling water mass flow through the electrolyser, where $\dot{m}_{cw,HT}$ and $\dot{m}_{cw,MT}$ show the mass

flow of cooling water directed towards the high-temperature and medium-temperature DHN application. The heating demand provided to the heat pump and heat exchanger are respectively denoted as Q_{HP} and Q_{HEX}.

3. Discrete operational decision variables that monitor the state of certain components are x_e, denoting the on/off status of the electrolyser, and x_{ch} and x_{disch} that monitor whether the battery is either charging or discharging.

As can be deduced from the previous enumeration, not all component sizes and working powers visible in Figure 2.1 are decision variables. For one, the dry cooler is always installed and is therefore not a decision variable. Further, the size of the hydrogen storage is determined by the daily amount of produced hydrogen and is therefore fixed when the objective is selected. Also, the hydrogen compressor size is not a decision variable, as its size is dependent on the electrolyser size. The same holds for some operational variables: the PV power is determined by the solar irradiance and ambient temperature, and the compressor power is determined by the electrolyser power, which dictates the mass of hydrogen that is to be compressed at any timestep.

2.3 Required input

The input data to the model can be classified into boundary conditions and literature and manufacturer data. First, the boundary conditions of the system consisted of the weather data (total solar irradiance G, ambient temperature T_a), the cost profile of exported and imported electricity ($\pi_{el,exp}$ and $\pi_{el,imp}$ respectively) and the target of daily produced hydrogen $m_{H_2,obj}$. This further encompassed the price of medium- and high-temperature heat ($\pi_{MT,exp}$ and $\pi_{HT,exp}$ respectively). The weather data and cost profiles were given for a horizon of one year, with an hourly resolution. Finally, the boundary conditions also covered the temperature levels at which the heat recovery system works.

Second, the literature and manufacturer data included the data for the installation cost (curves) of all components, as well as their maintenance costs, efficiency and lifetime. It also comprised all physical constants that were used in the modelling process, such as the higher heating value of hydrogen. The following subsections will detail the approximation of the component cost and efficiency curves as implemented in this model. Moreover, Section 3 details the input data for the case study used in this work.

2.3.1 Component cost

As mentioned in Section 1.3, the cost curve of system elements was taken into account for a more accurate description of equipment cost. These curves were introduced in the MILP by adding piecewise affine constraints that approximate the curve [23]. As this adds to the amount of decision variables and computational effort required to run the model, implementing component cost curves was done only for the compressor and electrolyser, since both experience large unit price reductions as their size increases [15]. The electrolyser cost curve reported by Reksten et al. [15] is implemented, whereas

the compressor cost is found in Minutillo et al. [2]. Both curves are concave functions that have to be minimized and therefore, binary variables were introduced to determine the active section of the PWA approximation. They are denoted as y_i, with i being the section number, and l is equal to the total number of sections in the PWA approximation. Only one of the binary variables y_i will have a value equal to one. Equations 2.1 - 2.3 denote the PWA constraints for the electrolyser cost, C_e, while the compressor cost (C_c) constraints are of equal syntax.

$$C_e = \sum_{i=1}^{l} (\alpha_i S_e + \beta_i)\, y_i \tag{2.1}$$

$$\sum_{i=1}^{l} y_i \leq 1 \tag{2.2}$$

$$\sum_{i=1}^{l} (y_i\, s_i) \leq S_e \leq \sum_{i=1}^{l} (y_i\, s_{i+1}) \tag{2.3}$$

In the above-mentioned equations, α_i and β_i are the coefficients that correspond to the linear sections of the piecewise approximation and s_i are the equipment sizes that correspond with the boundaries of each different section of the electrolyser size S_e.

As Equation 2.1 contains a bilinear term, this has to be rewritten in order for the MILP to remain linear. To this end, l auxiliary variables $\tilde{S}_{ey,i}$ were introduced, defined as follows:

$$S_e\, y_i = \tilde{S}_{ey,i} \tag{2.4}$$

$$S_{e,min}\, y_i \leq \tilde{S}_{ey,i} \leq S_{e,max}\, y_i \tag{2.5}$$

$$S_e - S_{e,max}(1 - y_i) \leq \tilde{S}_{ey,i} \leq S_e \tag{2.6}$$

In these equations, $S_{e,min}$ and $S_{e,max}$ respectively are the minimum and maximum size that constrain the electrolyser.

Thus, substituting $\tilde{S}_{ey,i}$ for the product $S_e\, y_i$ in Equation 2.1 gives the following (linear) equation for the electrolyser cost C_e:

$$C_e = \sum_{i=1}^{l} \alpha_i \tilde{S}_{ey,i} + \beta_i\, y_i \tag{2.7}$$

The number of PWA sections l was taken equal to 2 for the baseline scenario and the values for the variables α_i, β_i and s_i are given in Table 2.1 for both the electrolyser and compressor. For the electrolyser, a larger number of l was taken into account during the sensitivity analysis, where more extreme values for the electrolyser size can occur.

Table 2.1: Cost curve coefficients and variables for PWA approximation; denoted with * are the sizes and sections taken into account during the sensitivity analysis.

	α[kEUR/kW]	β [kEUR]	s_i [kW]
Electrolyser	{1.13*, 0.99, 0.92, 0.86*, 0.81*}	{63.93*, 100.57, 129.07, 162.65*, 197.03*}	{100*, 250, 400, 550, 850*, 1000*}
Compressor	{10.68, 8.15}	{59.28, 90.89}	{3, 18, 33}

2.3.2 Component efficiency

As done for the component cost curves, the component efficiency was modelled in detail. The PV and heat pump performance were calculated as exact values for every timestep, whereas the electrolyser and compressor performance were PWA approximations of thermoelectric models and experimental curves respectively. As the heat exchanger delivers heat passively to the MT DHN, its electrical performance is nonexistent and it is therefore not discussed in this Section. The constraints that govern its thermal performance are set forth in Section 2.4.2.

PV performance

The power generated by PV can be calculated as follows:

$$P_{PV} = G\,\eta_{cell}\,S_{PV} \tag{2.8}$$

where η_{cell} is the (constant) cell efficiency. As part of the objective of this thesis is the implementation of high-fidelity models, PV performance was also considered in this regard. Therefore, to compute the cell efficiency η_{cell} at a given point in time, the following equation was used [24]:

$$\eta_{cell} = \eta_{ref}\,(1 - \zeta_{ref}\,(T_{cell} - T_{ref}) + \gamma_{PV}\,log_{10}(G)) \tag{2.9}$$

Herein the parameters ζ_{ref} and γ_{PV} respectively represent the temperature and solar radiation dependency of the cell efficiency. They are both material properties and for crystalline silicone modules have values around 0.004 K and 0.12 respectively [24]. Further, η_{ref} is the efficiency of the PV module at the reference temperature T_{ref}, which in this report is taken as 0.15 at a temperature of 25 °C [25]. The actual cell temperature, T_{cell}, is given by the following equation:

$$T_{cell} = T_a + (NOCT - 20)\,\frac{G}{800} \tag{2.10}$$

in which T_a represents the ambient temperature. Another parameter required to determine the cell efficiency is the nominal operating cell temperature (NOCT) which is usually given by the cell manufacturer. The value is determined at an irradiance of 800 W/m^2, an ambient temperature of 20 °C and under no-load conditions. For monocrystalline and polycrystalline cells, the NOCT is approximately 45 ± 2 °C and

therefore, as no specific PV manufacturer is chosen, the value of 45 °C is used in this work for the NOCT. [26]

Using the equations and constants above in combination with an input of measurements for the ambient temperature and solar irradiance, the efficiency of the solar panels was calculated for every timestep t in the time horizon.

Electrolyser performance

To approximate the electrolyser performance, a high-fidelity model developed by Gabrielli et al. [19] was used. The model was adapted to account for an electrolyser working temperature of 70 °C and to use the higher heating value (HHV) of hydrogen to calculate the electrolyser efficiency. As argued in previous works [14, 21, 27], the use of the HHV of hydrogen in the efficiency gives a better estimate for the heat that can be recovered from the electrolyser.

The performance of the electrolyser is given by the curves in Figure 2.2. Figure 2.2a shows the electrolyser efficiency, where Figure 2.2b shows the normalized output power of the electrolyser. Since the electrolyser never operates below 20% of its nominal power, the curve was approximated between this value and 107% of its nominal power, the upper boundary calculated in [1]. A standby state of the electrolyser is not taken into account, as there is little literature on standby power consumption. Additionally, the modelling is done with an hourly resolution and thus cold startup effects are neglected [28]. However, due to the negative impacts of cold startup on electrolyser degradation and lifetime, a penalization cost is introduced to limit its occurrence, explained further on in Section 2.5.

The number of breakpoints on the curve is denoted by the letter n. A value of n equal to 1 means a constant efficiency for the electrolyser is assumed and thus the input-output power curve is approximated by a line through the origin and the single break point, whereas a value of n greater than 1 denotes an affine approximation of the curve. The accuracy of the approximation increases with an increasing value for n, as displayed in Figure 2.2c, which shows the relative error of the PWA approximation with respect to the high-fidelity curve.

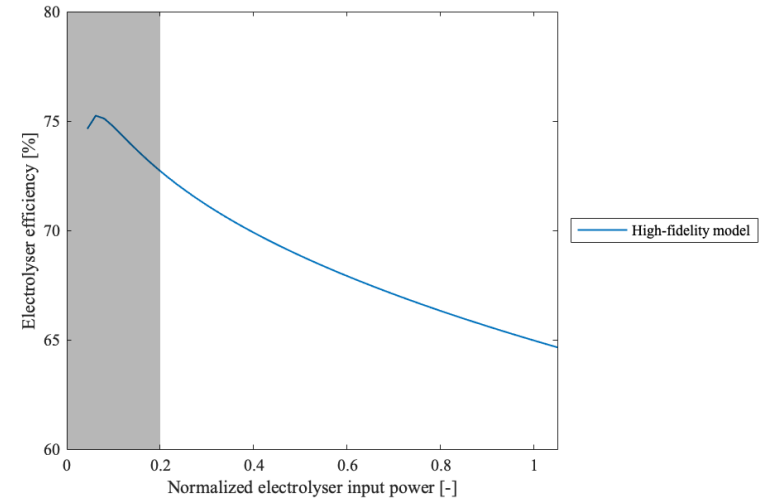

(a)

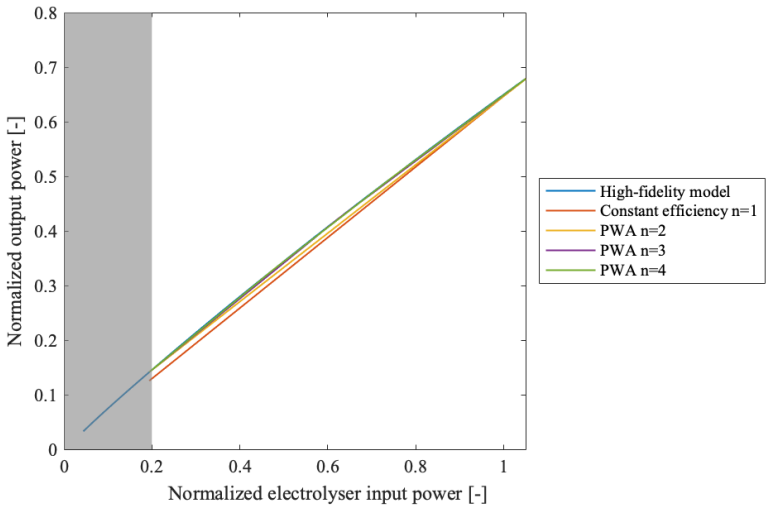

(b)

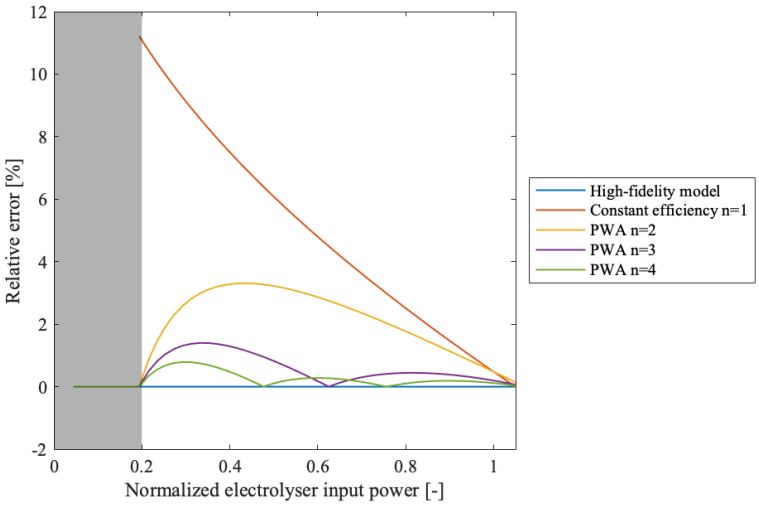

(c)

Figure 2.2: (a) Electrolyser efficiency curve given by a high-fidelity model [1]; (b) Normalized electrolyser output power as a function of the normalized input power: high-fidelity model [1] and piecewise affine approximations of different degrees; (c) Relative error of PWA approximations of the electrolyser efficiency.

To implement this efficiency curve in the model, the electrolyser output power was written as a function of the input power in Equation 2.11. Since the input-output curve is a concave curve that has to be maximized, no binary variables were introduced to determine the active section j of the PWA approximation, which is beneficial to the model solving speed.

$$P_{H_2} \leq \omega_j \, P_e + \varepsilon_j \, S_e \, x_e, \forall j \in [1, n-1] \tag{2.11}$$

wherein the coefficients ω_j and ε_j correlate the input and output power of the electrolyser for every section j and differ depending on the amount of breakpoints on the high-fidelity curve. The values for the different ω_j and ε_j are listed in Table 2.2. Furthermore, Table 2.2 also notes the average relative error of the PWA approximation.

x_e is a binary variable introduced in the beginning of this section and represents whether or not the electrolyser is switched on at a timestep t. Since bilinear terms cannot be handled by the MILP directly, an additional variable was again introduced as the product of S_e and x_e, called $\tilde{S}_{e,t}$. With the introduction of the new variable, the following additional constraints were necessary:

$$S_e x_e = \tilde{S}_{e,t} \tag{2.12}$$

$$0 \leq \tilde{S}_{e,t} \leq S_{e,max} \, x_e \tag{2.13}$$

$$S_e - S_{e,max} \, (1 - x_e) \leq \tilde{S}_{e,t} \leq S_e \tag{2.14}$$

Using the above equations, expressions are formed to calculate the electrolyser efficiency at every point in time.

Table 2.2: Electrolyser efficiency curve coefficients for PWA approximations with different numbers of break points and average relative error

	ω	ε	error
Constant	0.6269	//	4.91%
n = 2	0.6269	12.60	2.06%
n = 3	{0.65, 0.60}	{0.01, 0.05}	0.59%
n = 4	{0.67, 0.63, 0.59}	{0.01, 0.03, 0.05}	0.27%
n = 7	{0.68, 0.65, 0.63, 0.62, 0.60, 0.59}	{0.01, 0.02, 0.03, 0.04, 0.05, 0.06}	0.07%
n = 10	{0.68, 0.66, 0.65, 0.64, 0.63, 0.61, 0.60, 0.59, 0.59}	{0.01, 0.01, 0.02, 0.03, 0.03, 0.04, 0.05, 0.06, 0.06}	0.03%

Compressor performance

For the modelling of the compressor performance, the experimental curve reported by Timo Laaksonlaita was used [29]. The curve describes the approximated efficiency of a 900 bar piston compressor. The model does not distinguish between different compressor speeds and computes the compressor power as:

$$P_c = \dot{m}_{H_2} \, 2.5470 \frac{kWh}{kg} \tag{2.15}$$

The mass flow of hydrogen $\dot{m}_{H2}$ in kg/h is calculated from the electrolyser output power as follows:

$$\dot{m}_{H_2} = \frac{P_{H_2}}{HHV_{H_2}} \tag{2.16}$$

Heat pump performance

In order to calculate the power consumption of the heat pump, the coefficient of performance (COP) of the heat pump has to be known. This value indicates how much electric power is used by the heat pump to upgrade heat from a low-temperature reservoir to a high-temperature reservoir. As the temperature levels in the waste heat recovery system were constant, the COP is assumed in this work to have constant value. Therefore, it did not have to be approximated by a PWA function, but is expressed by Equation 2.17 below.

$$P_{HP} = \frac{Q_{HP}}{COP} \tag{2.17}$$

The theoretical maximum value that can be achieved for the COP of a heat pump, is its Carnot value [14], equal to:

$$COP_{carnot} = \frac{T_H}{T_H - T_C} \tag{2.18}$$

Where T_H and T_C are the temperatures of the high- and low-temperature reservoirs respectively. In this case, they corresponded to the supply temperature of the high-temperature DHN ($T_{HT,sup}$) and the cooling water temperature at the inlet of the heat pump (T_{out}). Filling out these values, the Carnot COP for the heat pump becomes:

$$COP_{carnot} = \frac{T_{HT,sup}}{T_{HT,sup} - T_{out}} \tag{2.19}$$

However, this is a theoretical maximum that cannot be achieved in actual heat pumps. Therefore, a reasonable approximation is to take the actual value of the COP to be half its ideal value [14, 30]:

$$COP_{real} = 0.5\, COP_{carnot} \tag{2.20}$$

2.4 Constraints

In this section, the constraints that govern the operation and sizing of the hydrogen generation site and waste heat recovery system are set forth. First, the energy balances characterizing the hydrogen generation and energy supply are explained. Second, the constraints that determine the working of the heat recovery system are detailed.

2.4.1 Hydrogen generation and energy supply

The primary goal of the site is to deliver a set sum of H_2 on a daily basis [2, 3]. The actual value of hydrogen produced in a day, $m_{H_2,prod}$, is thus subject to the following constraint:

$$m_{H_2,obj} \leq m_{H_2,prod} \leq 1.1\, m_{H_2,obj} \tag{2.21}$$

The upper boundary to the hydrogen production was introduced in order to avoid cases where more hydrogen is produced when it is convenient to sell heat or when there is an abundance of PV-generated power. Moreover, the hydrogen storage is sized to only contain the daily hydrogen objective and therefore larger amounts of hydrogen should not be produced.

As mentioned in Section 2.3.2, the minimum electrolyser power was set to 20% of the nominal power, as lower partial loads compromise safe electrolyser operation [16]. The constraint is implemented as follows:

$$0.2\, S_e\, x_e(t) \leq P_e(t) \leq S_e\, x_e(t) \tag{2.22}$$

the use of the auxiliary variable $\tilde{S}_{e,t}$, introduced in Section 2.3.2, is again necessary to avoid bilinear constraints. Further, thermodynamics dictates that no more energy can be delivered to the system than is used up by the system components. In Equation 2.23, the used energy is on the left-hand side of the equation and the delivered energy is on the right-hand side.

$$P_e + P_c + P_{HP} + \frac{P_{b,ch}}{\eta_b} + P_{exp} = P_{PV} + P_{b,disch}\,\eta_b + P_{imp} \tag{2.23}$$

Here η_b is the battery efficiency, a constant. There was an attempt to model the performance of the battery, but the non-linearity of the equations could not be worked away. The full attempt at incorporating this feature can be found in Appendix A.

Additional equations are necessary to model the working of the battery. First, it is decided that the battery can only be charged by solar PV, therefore the following equation needs to hold:

$$\frac{P_{b,ch}}{\eta_b} \leq P_{PV} \tag{2.24}$$

Secondly, the system can only be either charging or discharging at a certain point in time, so for all timesteps t, the following relation has to be respected:

$$x_{ch}(t) + x_{disch}(t) \leq 1 \tag{2.25}$$

Further, the energy stored by the battery is determined by the energy stored in the previous timestep, the charged power during the timestep and the discharged power in the timestep. No self-discharging has been taken into account.

$$E_b(t) = E_b(t-1) + P_{b,ch}(t)\,\Delta t - P_{b,disch}(t)\,\Delta t \tag{2.26}$$

Moreover, the energy stored in the battery is constrained between a minimum and maximum value of the state of charge (SOC), as shown in Equation 2.27. These values are 0.2 and 1 respectively, to account for realistic values that counteract accelerated battery degradation [16].

$$SOC_{min}\,K_b \leq E_b \leq SOC_{max}\,K_b \tag{2.27}$$

To ensure continuity of the system, the state of charge of the battery at the last timestep t_{end} should equal the state of charge in the first timestep at the beginning of the year:

$$SOC(t_1) = SOC(t_{end}) \tag{2.28}$$

Equation 2.26 can be enforced for all timesteps apart from $t = t_1$. Therefore, additional constraints at this initial state are required to comply with Equation 2.28, else an energy discrepancy would be found. Thus, both $P_{b,ch}$ and $P_{b,disch}$ should be equal to zero in this first timestep.

Lastly, both the charged and discharged power are constrained by the battery size and power rating, equal to 1C for both charging and discharging:

$$P_{b,(dis)ch} \leq \frac{K_b}{1\,h} \tag{2.29}$$

2.4.2 Heat recovery system

This section presents the system used to cool the electrolyser stack that operates at 70°C [1] and to recover this heat and deliver it to the district heating network at two temperature levels. The system and losses were designed in accordance with van der Roest et al. [21] and can be seen in Figure 2.3. The control of the heat recovery system is done by adjusting the mass flow of the cooling water in both the primary and secondary cooling loops to keep the temperature levels constant. At every timestep, the cooling water mass flow is described as follows:

$$\dot{m}_{cw} = \frac{P_e - P_{H_2}}{c_p\,(T_{HEX} - T_{in})} \tag{2.30}$$

Where c_p is the specific heat capacity of the cooling fluid, water in this case, equal to $4.186\,\mathrm{kJ/(kg\,K)}$.

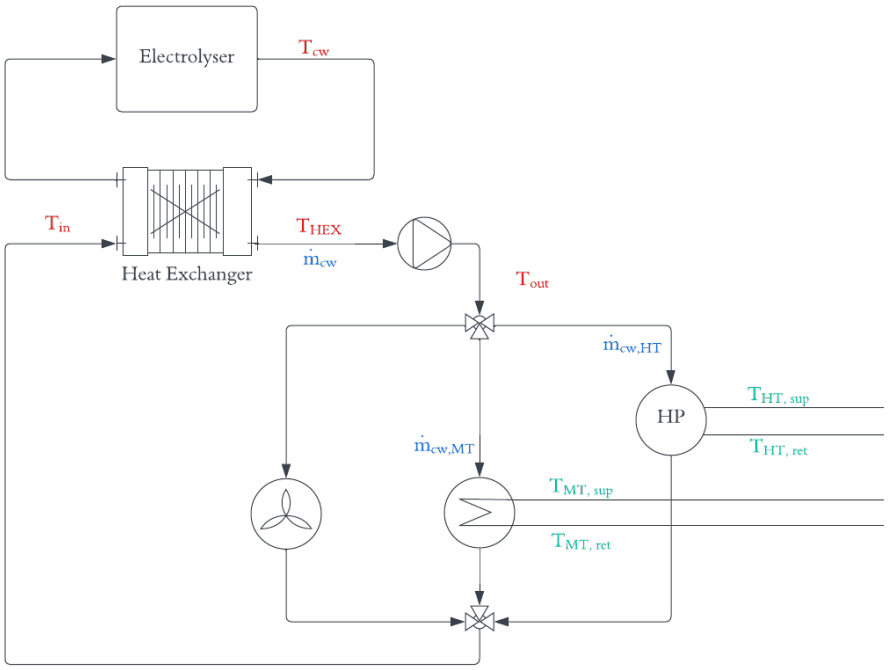

Figure 2.3: Schematic representation of the electrolyser heat recovery system, indicating the different temperature levels.

The cooling water is then redirected to the heat pump, heat exchanger or dry cooler (or a combination of all three):

$$\dot{m}_{cw,MT} + \dot{m}_{cw,HT} \leq \dot{m}_{cw} \tag{2.31}$$

As transport losses occur on the way to the heat delivery point, the heat degrades and the actual heat delivered to the HP and HEX are:

$$Q_{HP} \leq \dot{m}_{cw,HT}\, c_p\, (T_{out} - T_{in}) \tag{2.32}$$

$$Q_{HEX} \leq \dot{m}_{cw,MT}\, c_p\, (T_{out} - T_{in}) \tag{2.33}$$

The exact temperatures at which the heat is available are dependent on the Case Study and are further detailed in Section 3. The sizing of components and equations specific to the different district heating networks are described below.

The high-temperature DHN has a supply and return temperature of 66°C and 46°C [4]. Therefore, the electrolyser heat cannot be used directly to heat up the water, it first has to be upgraded to a higher temperature using a heat pump. The delivered heat cannot exceed the heat pump size:

$$Q_{HP} \leq S_{HP} \tag{2.34}$$

Additionally, it was assumed that the heat delivered to the high-temperature DHN is equal to the heat transferred by the cooling water:

$$Q_{DHN,HT} = Q_{HP} \tag{2.35}$$

The power required to run the heat pump was calculated as discussed in Section 2.3.2.

The medium-temperature DHN has a supply and return temperature of 36°C and 26°C respectively. Thus, using only a heat exchanger to deliver heat to the DHN is possible. Since the investment and operational costs of a heat exchanger are below those of a heat pump, this can be a favourable setup. The thermal power of the cooling water was calculated as follows:

$$Q_{HEX} \leq S_{HEX}\, U_{HEX}\, \Delta T_{lm} \tag{2.36}$$

Wherein U_{HEX} is the overall heat transfer coefficient of the heat exchanger, S_{HEX} is the area (in m^2) and ΔT_{lm} is the logarithmic mean temperature difference over the heat exchanger, calculated as [31]:

$$\Delta T_{lm} = \frac{(T_1 - T_4) - (T_2 - T_3)}{\ln \frac{(T_1 - T_4)}{(T_2 - T_3)}} \tag{2.37}$$

In this equation, T_1 is the inlet temperature of the hot fluid, which corresponds to the temperature T_{out} of the cooling water. Further, T_2 is the outlet temperature of the hot fluid, corresponding to T_{in}. Lastly, T_3 and T_4 are the inlet and outlet temperature of the cold fluid, namely the return and supply temperature of the medium-temperature DHN respectively ($T_{MT,ret}$ and $T_{MT,sup}$). As the mass flow of the cooling water throughout the loop is dynamically adjusted, the logarithmic temperature difference is constant.

As for the heat pump, it was assumed that no losses occur over the heat exchanger and all the heat delivered by the cooling water is delivered to the medium-temperature DHN:

$$Q_{DHN,MT} = Q_{HEX} \tag{2.38}$$

2.5 Objective function

The objective function of the MILP is the minimization of the total annualized cost C_{tot}, consisting of an annualized investment cost ($C_{inv,ann}$), a maintenance cost (C_{maint}), an operational cost (C_{op}) and a startup cost (C_{start}) as:

$$C_{tot} = C_{inv,ann} + C_{maint} + C_{op} + C_{start} \tag{2.39}$$

The annualized investment cost is expressed as the sum of the individual components' annualized capital cost:

$$\begin{aligned} C_{inv,ann} = {} & UP_{PV}\, P_{PV,peak}\, a_{PV} \;+\; UP_b\, K_b\, a_b + C_e\, a_e \;+\; UP_{HP}\, S_{HP}\, a_{HP} + \\ & UP_{HEX}\, S_{HEX}\, a_{HEX} \;+\; C_c\, a_c \;+\; UP_{stor}\, a_{stor} \;+\; UP_{refr}\, P_{refr}\, a_{refr} \;+\; UP_{disp}\, a_{disp} \end{aligned} \tag{2.40}$$

In which UP_ι is the unit price of a component ι and a_ι is the annuity factor for every component, calculated as:

$$a_\iota = \frac{d}{1-(d+1)^{l_\iota}} \tag{2.41}$$

As the annuity factor takes into account the individual components' lifetime l_ι and not the plant lifetime, no replacement costs need to be taken into account. The discount rate d is taken at 4%, as encouraged by the European Council for an Energy Efficient Economy in Energy Modelling [32].

Further, the maintenance cost for each component is determined as a fraction ξ_ι of the capital cost of the component ι. However, due to limited literature on maintenance costs of the components, this definition could not be applied for all and thus the maintenance cost is calculated as a fraction of the annualized capital cost in some of the cases, as detailed below:

$$\begin{aligned} C_{maint} = UP_{PV}\, P_{PV,peak}\, \xi_{PV} \;+\; UP_b\, K_b\, a_b\, \xi_b + C_e\, \xi_e \;+\; UP_{HP}\, S_{HP}\, a_{HP}\, \xi_{HP} \;+ \\ UP_{HEX}\, S_{HEX}\, a_{HEX}\, \xi_{HEX} \;+\; C_c\, \xi_c \;+\; UP_{refr}\, P_{refr}\, \xi_{refr} \;+\; UP_{disp}\, \xi_{disp} \end{aligned} \tag{2.42}$$

Lastly, the operational cost encompasses the expenses for imported energy, as well as the revenues generated by exporting electricity to the grid and heat to the medium- or high-temperature DHN. The cost is computed as the sum over all timesteps of the product of the imported or exported power with its unit price at every timestep. In Equation 2.43 expenses are denoted as positive, whereas revenues are appointed a negative sign.

$$\begin{aligned} C_{op} = \sum_{t=1}^{t_{end}} P_{imp}(t) \cdot \pi_{el,imp}(t) - \sum_{t=1}^{t_{end}} P_{exp}(t) \cdot \pi_{el,exp}(t) - \sum_{t=1}^{t_{end}} Q_{DHN,MT}(t) \cdot \pi_{MT,exp}(t) \\ - \sum_{t=1}^{t_{end}} Q_{DHN,HT}(t) \cdot \pi_{HT,exp}(t) \end{aligned} \tag{2.43}$$

The startup cost of the electrolyser is introduced in order to limit the amount of harmful startups of the electrolyser. Therefore, a penalty ν_{start} is charged for every electrolyser startup. The value of ν_{start} is 17 EUR, equal to the average cost of shutdowns shorter than one hour identified in [16].

An important parameter that can be derived from the objective function is the levelized cost of hydrogen (LCOH). It is recommended to calculate the LCOH as follows [33]:

$$LCOH = \frac{C_{inv,ann} + C_{maint} + C_{el,imp}}{\sum m_{H_2,prod}} \tag{2.44}$$

where $C_{el,imp}$, the cost of imported electricity required for the production of hydrogen, is taken into account.

However, in order to capture the value added by a waste heat recovery system to the hydrogen generation site, a different parameter is introduced. The value-adjusted levelized cost of hydrogen (VALCOH) is defined in Equation 2.45, taking into account the revenues generated by heat recovery from the electrolyser and from exporting electricity in the term C_{op}.

$$VALCOH = \frac{C_{inv,ann} + C_{maint} + C_{op}}{\sum m_{H_2,prod}} \tag{2.45}$$

The definition of the VALCOH as given above, corresponds to the metrics used in [2, 27], with the only difference that the term is not called LCOH, but rather VALCOH. Additionally, it is important to stress that with the current definition of the objective function, the system is optimized for minimal total annual cost and therefore minimal VALCOH. Optimizing for minimal LCOH would give results different to what is found with the current formulation.

The values for the unit price, lifetime and maintenance fraction of all components can be found in Appendix B, along with other techno-economic parameters.

2.6 Model contributions

The contributions of the current thesis to the reference optimization framework developed in [3] are shown in Table 2.3.

Table 2.3: Contributions of the current model relative to the reference from [3].

	Reference model	New model
PWA approximation of PV efficiency	✗	✓
PWA approximation of electrolyser efficiency	✗	✓
PWA approximation of compressor efficiency	✗	✓
PWA approximation of battery efficiency	✗	✗
Discrete sizing electrolyser	✓	✗
Discrete sizing battery	✓	✗
Continuous sizing electrolyser	✗	✓
Continuous sizing battery	✗	✓
Modelling WHR loop	✗	✓
Usage of Gurobi as a solver	✗	✓

2.7 Sensitivity analysis

In order to assess the influence of a parameter on the optimal result, a sensitivity analysis was performed. In the sensitivity analysis of models for multi-energy systems, it is common practice to vary input variables and assess the effect on the objective function. The choice of these variables, however, is not often based on the outcome of a broader

global sensitivity analysis (GSA). Therefore, a GSA was performed in this thesis to determine which individual inputs were looked at in more detail.

2.7.1 Global sensitivity analysis

The chosen global sensitivity analysis is the Morris screening method. This method was chosen as it can handle a large number of parameters for computationally expensive models with a relatively small number of model evaluations [34, 35]. As variance-based techniques would be too computationally expensive, this elementary effects method is suitable for determining which of the input parameters the model is most sensitive. The method works by calculating the elementary effects of q input parameters $(u_1, ..., u_q)$ on the model output $f = f(u_1, ..., u_q)$, varying the inputs one at a time. k sampling points are taken per input, which in this work was done by Latin hypercube sampling [36]. The model output that was considered is the value for the objective function. The elementary effect (EE) for the pth input at the kth sampled location, with an increment δ in the hyperspace, is calculated as follows [37]:

$$EE_p^{(k)} = \frac{f\left(u_1^{(k)}, ..., u_{p-1}^{(k)}, u_p^{(k)} + \delta, u_{p+1}^{(k)}, ..., u_q^{(k)}\right) - f\left(u_1^{(k)}, ..., u_q^{(k)}\right)}{\delta} \tag{2.46}$$

The mean value μ of the EEs of an input parameter reflects the overall effect of the parameter on the model output. The standard deviation σ of the EEs assesses the the parameter's non-linear effects and interactions with other inputs. Equations 2.47 and 2.48 respectively define these parameters for each input p.

$$\mu_p = \sum_{r=1}^{k} |EE_p^{(r)}|/k \tag{2.47}$$

$$\sigma_p = \sqrt{\sum_{r=1}^{k} |EE_p^{(r)} - \mu_p|^2/k} \tag{2.48}$$

Both factors should be considered simultaneously, since input parameters with elementary effects of a different sign would result in a low value of μ, but a larger value for σ [35]. Hence, type II errors can occur when μ and σ are not both taken into account.

2.7.2 Sensitivity analysis on individual parameters

As a second part of the sensitivity analysis, parameters that were found to have a large influence in the GSA were looked into individually in more detail to better understand how they affect the outcome of the optimizer. Here, not only the total cost was looked into, but the full breakdown of costs, the VALCOH and the added value of waste heat recovery.

Chapter 3

Case Study

This chapter presents the case study to which the model, described in Chapter 2, is applied. The studied case is that of the Swiss Federal Laboratories for Materials Science and Technology (Empa) on its campus in Dübendorf, Switzerland.

Specific to the case is also the value for the objective of produced hydrogen $m_{H_2,obj}$, taken as 100 kg/day [2]. Further, both the battery charging and discharging efficiencies η_b have an assumed value of 0.92 [16]. Moreover, the values for the unit price, lifetime and maintenance fraction of all components as used in Section 2.5 can be found in Appendix B.

3.1 Input data

The weather and cost data used in this case study as input to the model are historical data from Dübendorf, Switzerland in the year 2022 and are shown in Figure 3.1 for the relevant time horizon of one year [4,38,39]. The cost of imported electricity is calculated as the day-ahead price, plus the transmission fees. The latter are equal to the sum of the taxes, reactive power control and grid usage fees as applied by Glattwerk AG for a C6 demand profile. It is worth noting that the electricity price in 2022 was very high, with the average cost of imported electricity at 0.37 EUR/kWh, a stark contrast to the 0.14 EUR/kWh recorded in 2018. Further, the price of medium and high-temperature heat depicted in the Figure are determined as a fraction of the price of imported electricity [40]. The used fractions are dependent on the time of year, as suggested by Baldini, and can be found in Table 3.1.

Table 3.1: Weighting factors for the calculation of exported heat prices.

	Winter	Shoulder season	Summer
High temperature DHN	0.432	0.306	0.137
Medium temperature DHN	0.240	0.107	-0.025

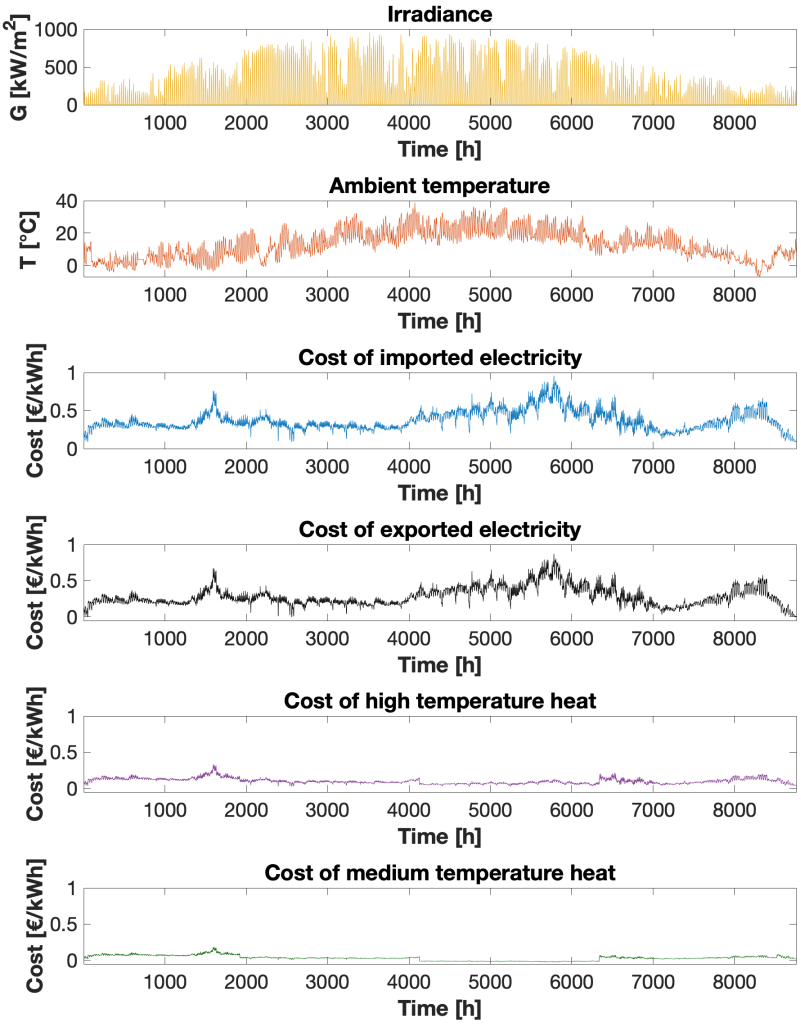

Figure 3.1: Summary of all weather and cost data used as model inputs.

3.2 Heat recovery system

The heat recovery system described in Section 2.4.2 operates at certain temperature levels. An operating temperature of 70 °C is chosen for the electrolyser [1] and the temperature losses in the primary and secondary cooling loops are analogous to the ones in the paper by van der Roest as shown in Figure 3.2 [21]. The temperature of the cooling water exiting the electrolyser is 67°C (T_{cw}), a 3°C temperature difference with the electrolyser operating temperature present. Further, the cooling water re-entering the electrolyser is at 60°C after the heat exchanger. In the secondary cooling loop, the outlet temperature after the primary heat exchanger is 64°C (T_{HEX}) and the inlet temperature (T_{in}) is equal to 57°C. Along the piping to the heat pump and heat exchanger for delivering heat to the DHNs, heat losses are taken into account by a decrease in cooling water temperature. A decrease of 2°C is assumed, hence the temperature of the water when it reaches the heat pump or heat exchanger is equal to 62°C (T_{out}).

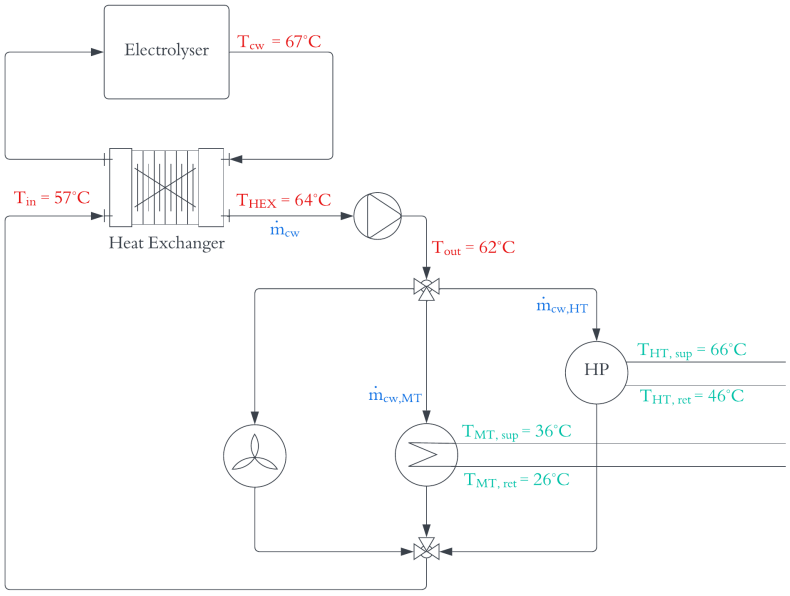

Figure 3.2: Schematic representation of the electrolyser heat recovery system, noting the different operating temperatures.

The assumed efficiencies for the heat recovery system are verified against data from the electrolyser at MOVE, in Empa [41]. Due to limited experimental data from the MOVE demonstrator, only a verification of the heat recovery fraction was possible. Three hours of electrolyser operating data yields a mean value of the electrolyser power 168.75 kW as shown in Figure 3.3a. As the electrolyser nominal power is equal to 180 kW, this corresponds with a mean partial load fraction of 0.9375. The cooling water power is calculated using the cooling water supply and return temperature measurements, shown in Figure 3.3b, and the measured mass flow rate, visible in Figure 3.3c. At this level of

operation, the empirical heat recovery fraction at MOVE is calculated as follows

$$\phi_{rec,emp} = \frac{P_{th,emp}}{P_{e,emp}} = \frac{\dot{m}_{cw,emp}\,(T_{cw,ret,emp} - T_{cw,sup,emp})}{P_{e,emp}} \tag{3.1}$$

and yields a value of 0.3029.

The heat recovery fraction for the modelled electrolyser at the same average partial load as the electrolyser at MOVE is calculated next. For all possible values for n, the number of break points on the electrolyser efficiency curve, the electrolyser power at this partial load corresponds to the last section of the PWA approximation of the efficiency curve (section n-1). As the electrolyser is switched on by default in order to assess the heat recovery, x_e will equal 1 and the expression for the electrolyser output becomes:

$$\begin{aligned} P_{H2} &= \omega_j\, P_e + \varepsilon_j\, S_e\, x_e \\ &= \omega_{n-1}\, 0.9375\, S_e + \varepsilon_{n-1}\, S_e \\ &= \left(0.9375\, \omega_{n-1} + \varepsilon_{n-1}\right) S_e \end{aligned} \tag{3.2}$$

Thus, the heat recovery fraction is computed as follows:

$$\begin{aligned} \phi_{rec} &= \frac{P_{th}}{P_e} = \frac{P_e - P_{H2}}{P_e} \\ &= 1 - \frac{P_{H2}}{P_e} \\ &= 1 - \frac{\left(0.9375\, \omega_{n-1} + \varepsilon_{n-1}\right) * S_e}{0.9375 * S_e} \\ &= 1 - \omega_{n-1} - \varepsilon_{n-1}/0.9375 \end{aligned} \tag{3.3}$$

For different values of n, this recovery fraction ranges from 0.3460 to 0.3475. Thus, the model estimates that roughly 4% more heat is recovered than what is the case in the electrolyser at MOVE. As the simulated electrolyser model does not correspond with the installed electrolyser at MOVE, and neither does the installed power, this difference is accepted.

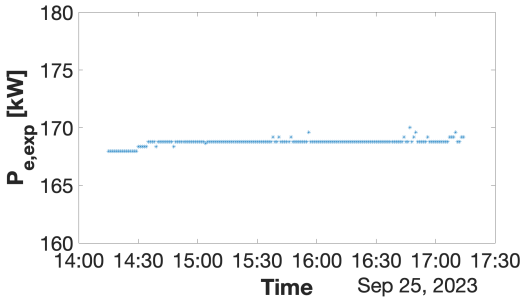

(a) MOVE electrolyser power

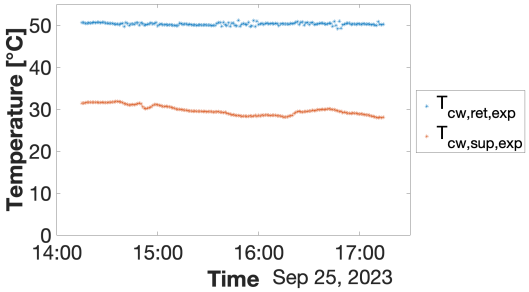

(b) MOVE cooling water supply and return temperatures

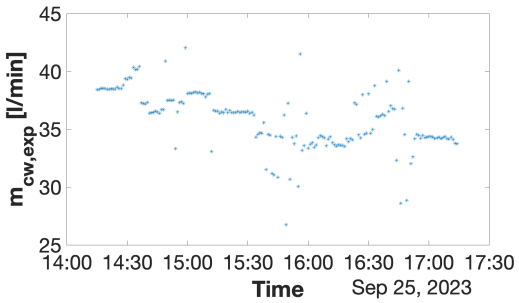

(c) MOVE cooling water mass flow

Figure 3.3: Experimental data from the electrolyser at the MOVE demonstrator.

Chapter 4

Results and Discussion

In this chapter, the most important results are discussed. First, the influence of the PWA approximation of the electrolyser efficiency on both the optimal system layout and operation is quantified. Moreover, a value for n, the number of break points on the electrolyzer efficiency curve, is selected for the baseline scenario, with which all the consequent calculations are done. Second, the waste heat recovery profile is looked at in detail, denoting seasonal changes and overall values. Further, the costs of a system with and without WHR are examined, as well as their VALCOH. Last, a sensitivity analysis is performed on the model parameters: on the one hand a GSA to determine relevant parameters, on the other hand a detailed study of individual parameter's influence on component sizing, VALCOH and WHR.

4.1 Reference scenario

As introduced in Section 2.3.2, the efficiency of the electrolyser is approximated by a PWA function to increase the level of fidelity of the model. The effect of the level of accuracy on the optimal component sizing is illustrated in Table 4.1 for approximations by a constant electrolyser efficiency, or PWA with 2, 3, 4, 7 and 10 break points on the efficiency curve. The table demonstrates that several factors are constant over the different levels of accuracy: the PV power is always maximized, a battery is never selected to even out PV intermittence and the heat recovery system comprises of a heat pump and not a heat exchanger. Furthermore, the relative change in component size and system cost quickly decreases with increasing accuracy. However, a significant difference of almost 10% is found between the electrolyser size for a constant efficiency approach and the chosen baseline scenario with n = 4 break points. The scenario with a value of 4 for n is chosen as the reference scenario as a trade-off between optimality and computational cost. Concretely, moving from the scenario with n = 4 to n = 7 the value for the objective function decreases by 0.17%, whereas the solver time increases by 345.45%, to eight hours and ten minutes. Therefore, to strike the balance between

Table 4.1: Optimal value for sizing decision variables and objective function at different levels of approximation of the high-fidelity electrolyser efficiency curve.

	$P_{PV,peak}$	S_e	S_{HP}	S_{HEX}	C_b	C_{tot}	VALCOH
Constant	+ 0%	- 9.95%	- 9.35%	+ 0%	+ 0%	+ 3.88%	+ 3.53%
n = 2	+ 0%	- 0.94%	- 0.27%	+ 0%	+ 0%	+ 1.68%	+ 1.69%
n = 3	+ 0%	- 0.43%	- 0.29%	+ 0%	+ 0%	+ 0.26%	+ 0.26%
n = 4	1500 kW	410.78 kW	102.81 kW	0 m^2	0 kWh	389.81 kEUR/y	10.65 EUR/kg
n = 7	+ 0%	- 0.04%	- 0.18%	+ 0%	+ 0%	- 0.17%	- 0.17%
n = 10	+ 0%	+ 0.12%	- 0.06%	+ 0%	+ 0%	- 0.22%	- 0.22%

limiting computational cost while retaining an accurate representation of electrolyser performance, the scenario with 4 break points is chosen as baseline.

Table 4.1 shows the optimal value of the main sizing decision variables and value for the objective function for the 'best approximation'. The relative difference between the final value of the decision variables for the chosen scenario and the scenarios with different levels of approximation is also tabulated.

The data in Table 4.1 can be compared to the values for the relative error in Table 2.2. In the scenario where constant efficiency is assumed, the electrolyser size is greatly influenced by the level of accuracy, as the difference in S_e is double the average error in output power. Where n=2, the difference in S_e with the reference case is 10 times smaller than for constant efficiency, although the error on the PWA approximation is merely 2.4 times lower. Thus, a large dependence of the electrolyser size on the PWA accuracy is found at approximation errors in the magnitude of 4%, whereas errors from 2% have lower influence on electrolyser size. Regarding the total cost and VALCOH, the consecutive relative difference across different values of n align with the errors from the PWA approximation.

The level of fidelity of the efficiency approximation not only influences the component sizing, but also their operation. To demonstrate these differences, the operation of the electrolyser is shown in Figure 4.1 for a horizon of one day, for the different curve approximations. The figure demonstrates how the use of partial load changes when more accurate approximations of the efficiency curve are used. The scenario with constant efficiency, as shown in Figure 4.1a, almost exclusively uses the electrolyser at full load or at minimum load, whereas when n = 10, many more working points in between are used and the operating curve becomes more smooth. Thus, ability to account for a higher electrolyser efficiency at partial load allows to more accurately predict hydrogen production and therefore lowers the VALCOH.

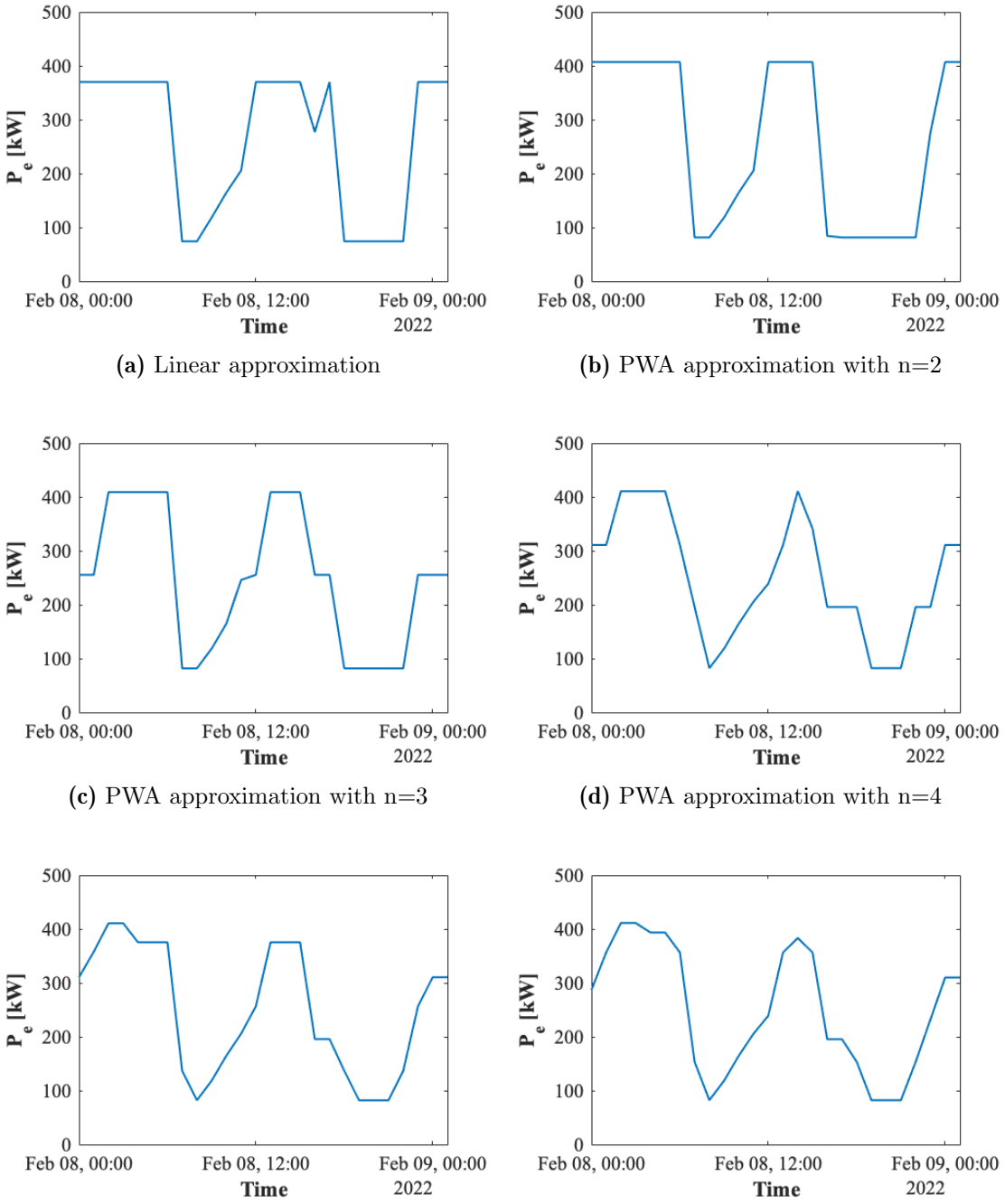

(a) Linear approximation

(b) PWA approximation with n=2

(c) PWA approximation with n=3

(d) PWA approximation with n=4

(e) PWA approximation with n=7

(f) PWA approximation with n=10

Figure 4.1: Electrolyser power profile for different levels of approximation of the high-fidelity electrolyser efficiency curve.

4.2 Waste heat recovery

The profile of the heat recovery from the electrolyser is shown in Figure 4.2, for one week in every season. As is clear from the choice of heat recovery equipment, heat is only exported to the HT DHN using a heat pump. This is done in every season of the year, but the recovery profile differs from season to season due to the changes in electrolyser operation with the seasons. In spring and summer, the electrolyser is used at nominal power more often than in autumn and winter, because of the large amounts of power generated by the solar panels during this time of year. In autumn and winter, the availability of PV-generated electricity is lower and thus the electrolyser operates more often at the partial loads, which have higher efficiency. Therefore, the total amount of heat that is recovered also depends on the season: approximately 4% more heat is recovered in summer than in winter, the two seasons with respectively the most and least recovery. As mentioned, this is due to the electrolyser working conditions: at full load and lower efficiency in summer, at partial load and higher efficiency in winter.

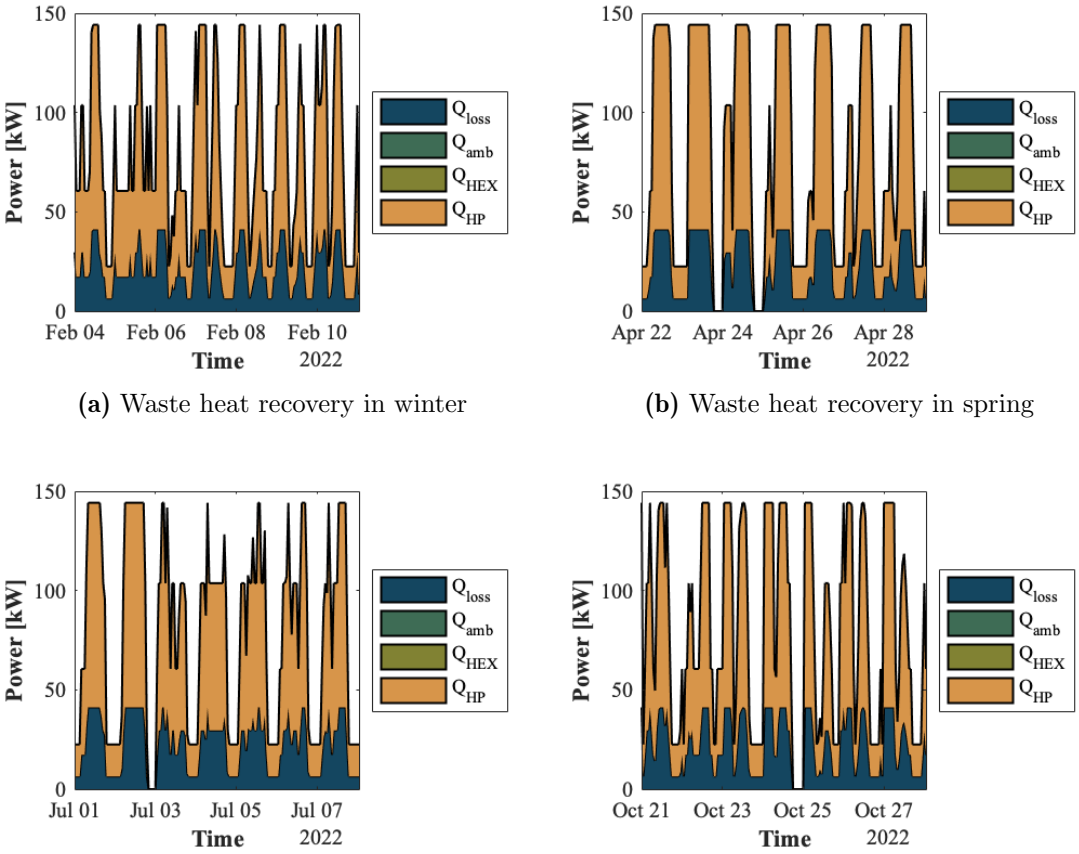

(a) Waste heat recovery in winter

(b) Waste heat recovery in spring

(c) Waste heat recovery in summer

(d) Waste heat recovery in autumn

Figure 4.2: Electrolyser waste heat recovery profile for four representative weeks, one in every season of the year.

4.3 Levelized cost of hydrogen

In this section, the comparison is made between an optimized system with and without waste heat recovery. On the one hand, the model developed in this thesis is used to simultaneously determine the optimal sizing and operation of the components in a system with and without WHR. On the other hand, the model is used to determine the optimal operation of an energy system where the size of the components is predetermined. For the latter, the sizing method of a reference paper [2] is followed for the PV area and the electrolyser. The electrolyser size is determined by assuming 24 hours of operation at full load to achieve the daily goal of 100 kg/day of produced hydrogen. Using the nominal electrolyser efficiency as given in Section 2.3.2, this results in an electrolyser size of 253 kW.

Optimizing the system for the stated conditions, with and without WHR, yields the results summarized in Figure 4.3 and 4.4. As shown in the first figure, the value-adjusted levelized cost of hydrogen, as defined in Section 2.5, is lower for the cases where heat recovery is implemented. More concretely, a decrease of 6.0% is observed for the full optimization, whereas the decrease in the case of the reference paper is 6.3%. This indicates that for systems with suboptimal component sizing, the benefits of implementing waste heat recovery are larger. A second observation from Figure 4.3 is that the VALCOH is lower in all scenarios where optimization of both size and operation of components was done, as opposed to the reference paper. Hence the importance of not only optimizing the plant operation, but also simultaneously optimizing the component size, is shown: concurrent optimization lowers the total costs. Overall, the comparison between the reference paper where no waste heat is recovered, and the optimization brought forward in this work yields an 18.9% decrease in VALCOH when implementing the concurrent optimization with WHR.

The total cost breakdown in Figure 4.4 demonstrates that the increase of investment and maintenance costs due to the addition of WHR does not weigh up to the increase in revenues generated by it. Further, for the partially optimized (reference paper) system, increased cost of imported electricity is the driver for a higher VALCOH. Due to the small electrolyser size, it cannot be operated at its more energy-efficient partial load and therefore, more electricity is required to produce the target amount of hydrogen.

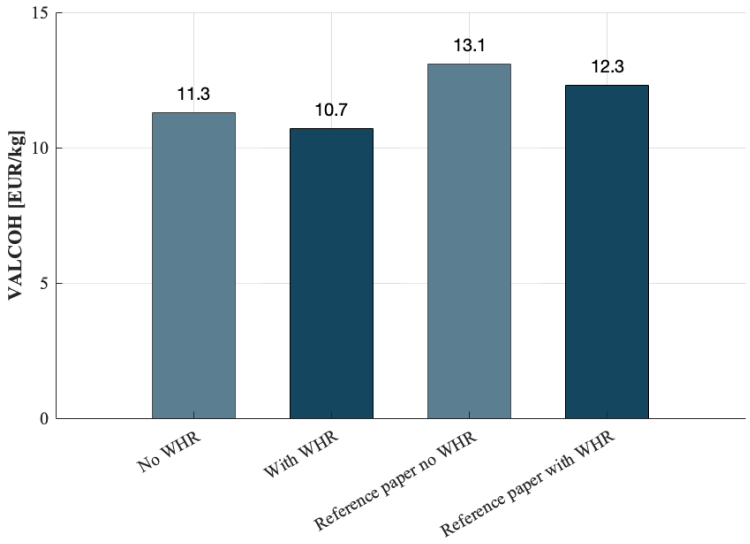

Figure 4.3: The levelized cost of hydrogen with and without considering waste heat recovery; for the case of a full system optimization, and the case of a partial optimization using the equipment sizing from a reference paper [2].

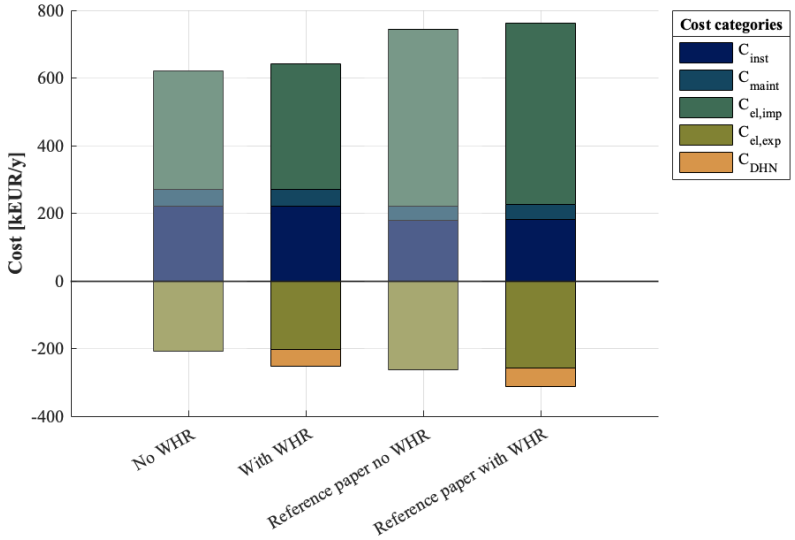

Figure 4.4: The breakdown of the total system's yearly cost with and without considering waste heat recovery; for the case of a full system optimization, and the case of a partial optimization using the equipment sizing from a reference paper [2].

4.4 Sensitivity analysis

In this chapter, a sensitivity analysis is performed on the results. First, a global sensitivity analysis is carried out using the Morris screening method as described in Section 2.7.1. The parameters that emerge as most sensitive from this analysis are then further looked at in more detail to have a better understanding of their effect on the objective function.

4.4.1 Global sensitivity analysis

Parameter values are sampled out of a uniform distribution of the values in the ranges defined in Table 4.2. The values in the table are relative to the nominal value of the parameter as given in Section 3.1 and Appendix B. It is decided to look into the following parameters for the sensitivity analysis: the electrolyser cost and lifetime, the heat pump cost and lifetime and the battery cost. Further, the electrolyser efficiency is looked at in more detail, since it has a large influence on the power required to produce hydrogen, but also on the heat recovery. Further, the area available for PV panels is expected to have an influence, as well as the discount factor and the temperature of the cooling water. Last, the influence of the cost of imported electricity (and consequently the price of exported heat) is investigated, as well as the electrolyser startup cost.

Table 4.2: Relative variation of parameters in the GSA, absolute variation of parameters denoted by *

	c_e	UP_{HP}	UP_b	l_e	l_{HP}	η_e*	$S_{PV,max}$	d	T_{out}*	$\pi_{el,imp}$	ν_{start}
Max variation	+ 20%	+ 20%	+ 20%	+ 100%	+ 100%	+ 20%	+ 100%	+ 20%	+ 5°C	+ 100%	+ 20%
Min variation	- 80%	- 80%	- 80%	- 50%	- 50%	- 10%	- 50%	- 80%	- 5°C	- 50%	- 80%

The elementary effects are calculated by the Morris method, detailed in Section 2.7.1, for the parameters above. The resulting mean values and standard deviations of the EEs are shown in Figure 4.5. Parameters that have a large influence on the objective function exhibit large mean values in their EEs. The standard deviations in their EEs speaks to the nonlinearity of their effect on the objective function. From the GSA, it is apparent that the electrolyser startup cost, the heat pump unit price and lifetime, as well as the battery unit price, exert minimal influence on the value of the objective function. Conversely, the available PV area has a very large influence. Modifying this parameter changes the amount of electricity that has to be imported from the grid to a large extent, affecting the operational costs. However, while acknowledging how sensitive the model is to this parameter, the focus of this thesis is on the heat recovery aspect and not the renewables. Thus, this parameter is not looked into further. Next, the electrolyser efficiency and the imported electricity prices notably influence the model output; and this is investigated in the following Section. The electrolyser cost emerges as another parameter that has a significant influence on the objective function, which is promising for the competitiveness of (green) hydrogen generated via electrolysis, as the learning rate for PEM electrolysers is estimated around 25-30% [15]. The developed model is

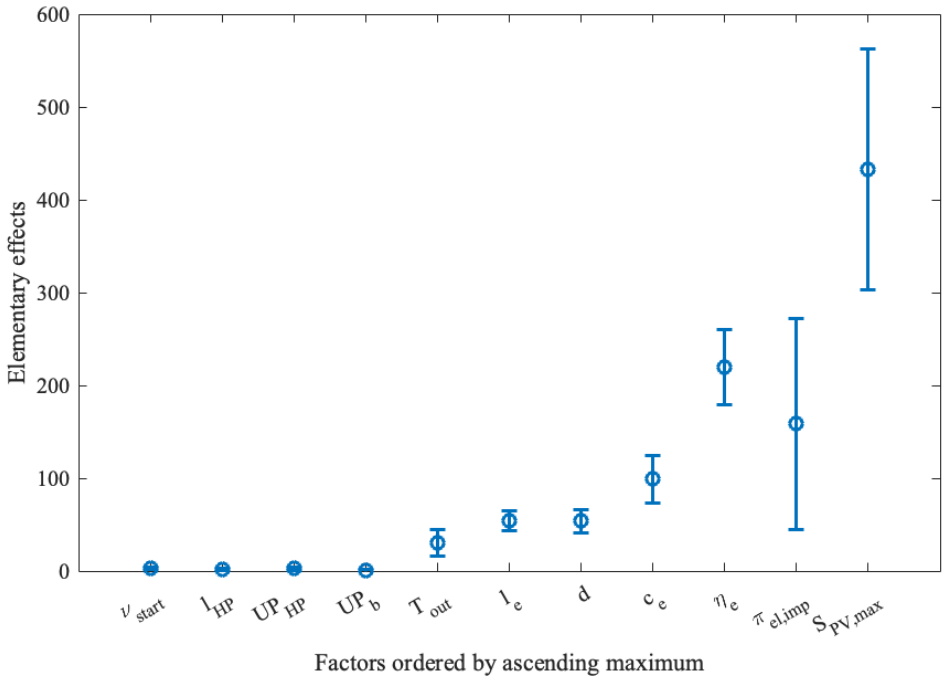

Figure 4.5: Elementary effects of the parameters in the GSA.

less sensitive towards the three remaining parameters: the discount rate, electrolyser lifetime and CW temperature. Therefore, due to their limited influence, the fact that the discount rate is out of the scope of the report and that changing the CW outlet temperature has implications on the electrolyser working temperature and efficiency; these factors are simply mentioned but not further explored.

4.4.2 Individual parameters

From the global sensitivity analysis, $\pi_{el,imp}$ and η_e are identified as relevant parameters to which the model is sensitive. Therefore, they will be explored first in this section, together with an analysis of the battery cost. Further, the mass of produced hydrogen is varied, while keeping the fraction of renewables constant. Subsequently, scenarios with specific heat demands are looked into to gain a complete understanding of all aspects of WHR to district heating networks.

Electricity cost

The cost of electricity emerged from the GSA as a parameter with a great influence on the objective function, and is looked at in more detail. Concretely, the optimization is run for the year 2018, a pre-covid scenario with electricity prices that are much lower than the year 2022. Additionally, the irradiation and temperature profiles are updated

Table 4.3: Optimization results for the main sizing decision variables for the year 2018 and 2022

Year	S_e [kW]	S_{HP} [kW]	S_{HEX} [m^2]
2018	314	79	0
2022	410	103	0
2022 + 50%	478	120	0

to the year 2018 to capture all aspects of different scenarios and the input data profiles are attached in Appendix C [38, 39]. The optimization is further also performed for the data in 2022, with a 50% increase in the cost of electricity, to mirror a potential future scenario.

Table 4.3 summarizes the sizes for the main components the three cases. As the cost of imported electricity is much lower in 2018, the optimizer chooses a smaller electrolyser to reach the same hydrogen production. Thus, the electrolyser will be working at higher partial loads throughout the year, generating more heat that can be recovered to the DHN. Figure 4.6 shows that although more heat is recovered from the electrolyser, less revenues are generated by the export of heat to the DHN due to its lower export price (calculated as a fraction of the electricity cost). The opposite is true for the 2022 scenario with higher electricity prices: a larger electrolyser allows for more benefits of working at partial load and even though less heat is recovered, more revenues are generated from the WHR.

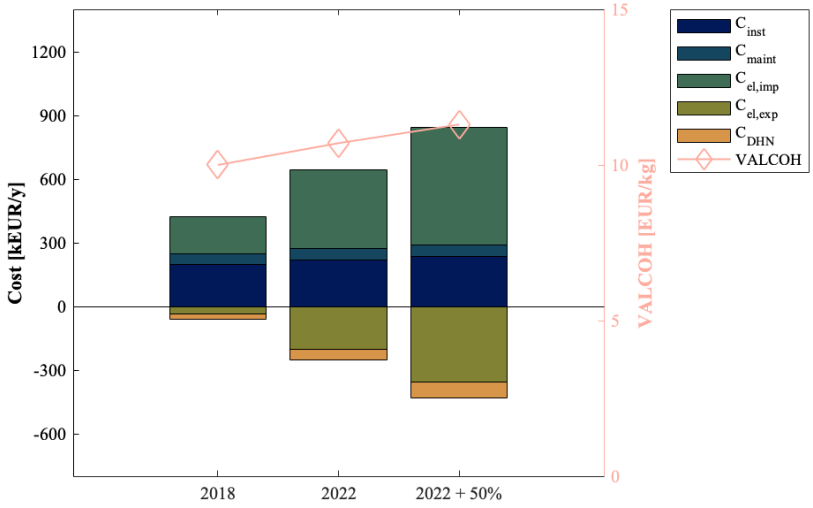

Figure 4.6: Summary of costs for the year 2018 and 2022; weight of cost categories on the left-hand axis and the VALCOH on the right-hand axis.

Overall for the year 2018, the value-adjusted levelized cost of hydrogen decreases by 6.3%, mainly due to the decrease in costs from imported electricity. Contrarily, the

Table 4.4: Optimization results for the main sizing decision variables for the scenarios with different electrolyser efficiency

η_e [-]	S_e [kW]	S_{HP} [kW]	S_{HEX} [m^2]
Baseline	410	103	0
+ 20%	297	32	0

VALCOH increases by 6.4% in the future scenario due to the increase in operational costs, the effect mainly attributed to the imported electricity as well.

Electrolyser efficiency

From the GSA it is evident that the electrolyser efficiency has a large influence on the total system cost. Therefore, this subsection looks more closely at its effect on component sizing and the breakdown of costs, by increasing the efficiency curve by an absolute 20%. The component sizing is outlined in Table 4.4, where it is shown that an increase in efficiency results in a decrease in electrolyser size. Additionally, the heat pump size decreases more than linearly with the decrease in heat pump size. This is due to the double effect of the increase in efficiency: first, the increase leads to a smaller heat pump merely because of the smaller electrolyser, but secondly, as the electrolyser works more efficiently, less heat is generated and thus an even smaller heat pump size is required.

Figure 4.7 shows the cost breakdown for the baseline and increased efficiency scenario, both with and without WHR implementation. Comparing the scenarios with WHR and different electrolyser efficiency, it can be seen that the decrease in VALCOH is due to multiple factors. The required electrolyser size is lower, thus the heat pump is smaller and overall investment and maintenance costs decrease. Further, the operational costs fall as less electricity is required to produce the hydrogen. Conversely, revenues from selling heat to the DHN decrease, as less heat is produced as by-product. Overall, the VALCOH falls by 40% when increasing the efficiency by 20%.

When inspecting the implementation of WHR in the system, it is noted that with an increased efficiency the benefit of adding a heat recovery system is lower than for the baseline scenario. As opposed to the 6% decrease in VALCOH by adding WHR to the baseline, the VALCOH only decreases by 3% in the case of increased efficiency. Nonetheless, there is still a benefit to be found in adding a heat recovery system. Conversely, the importance of implementing WHR will increase if the electrolyser efficiency decreases, as it does by degradation over time.

In the context of the sensitivity analysis, a 20% surge in efficiency is examined to shed light on the broader trends associated with this increase. It is noteworthy that this level of efficiency is not yet manifested in PEM electrolysers, however it is recorded for Solid Oxide Water Electrolysers [42].

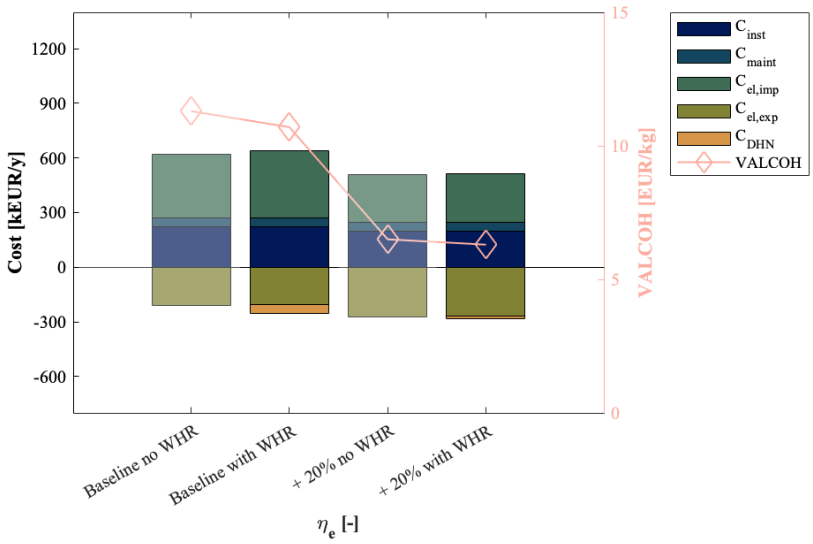

Figure 4.7: Summary of costs for the system with and without WHR for the baseline scenario and an increased electrolyser efficiency; weight of cost categories on the left-hand axis and the VALCOH on the right-hand axis.

Battery cost

As shown in the GSA, the system is not very sensitive to changes in battery cost. Moreover, not one of the investigated scenarios thus far has had a battery system implemented. Therefore, it is interesting to determine what value for the battery cost results in the optimiser choosing a battery. Using trial and error, a battery cost that ensures a non-zero size for the battery is found: $\mathrm{UP_b} = 110\,\mathrm{EUR/kWh}$. This value corresponds to a decrease in cost of over 80% versus the baseline. When the system is optimized with this unit price, an optimal battery size of 353 kWh is found. Over the time horizon of 1 year, the amount of energy charged to and discharged from the battery sums up to 78 MWh, resulting in a decrease of 3% in the amount of imported electricity compared to the baseline scenario. Furthermore, the VALCOH decreases to 10.63 EUR/kg, a 0.2% difference from the baseline. Therefore, a decrease in battery size by over 80% only yields a decrease in VALCOH of 0.2%, and a decrease of 3% in imported electricity. Thus the addition of a battery barely has an influence in how 'green' the produced hydrogen is, nor does it significantly lower the VALCOH.

Mass produced hydrogen

Another parameter that is investigated more closely as a part of the sensitivity analysis is the daily produced mass of hydrogen.Besides the baseline value of 100 kg/day, two other scenarios are looked at in more detail:

$$\mathrm{m_{H_2,obj}} = 200\,\mathrm{kg/day}$$

Table 4.5: Optimization results for the main sizing decision variables for the scenarios with different targets of produced hydrogen.

$m_{H2,obj}$ [kg/day]	S_e [kW]	S_{HP} [kW]	S_{HEX} [m^2]
200 kg	893	224	0
100 kg	410	103	0
50 kg	193	48	0

$$m_{H_2,obj} = 50\,kg/day$$

The system is optimized with those different values for the objective produced hydrogen ($m_{H2,obj}$), but the ratio of maximum PV area to the hydrogen objective is kept constant. The main components' sizes are summarized in Table 4.5. The electrolyser size increases almost linearly with increasing hydrogen targets and thus it is expected that the electrolyser operation profile is similar to the baseline scenario. The size of the heat pump increases/decreases by the same percentage value as the electrolyser size for both scenarios, whereas the heat exchanger is again not selected as a part of the heat recovery system.

Figure 4.8 summarizes the key cost findings for the different scenarios analyzed. Looking into the data, the installation and maintenance costs reveal clear benefits when installing components for a larger hydrogen production capacity, as can be expected due to economies of scale. As the ratio of installed PV capacity to hydrogen objective is kept constant, the imported and exported electricity costs more or less increase linearly with the increasing hydrogen target. The same holds for the heat exported to the DHN, meaning that the decrease in VALCOH is only because of economies of scale. Furthermore, the relative decrease in VALCOH from a system without WHR to a system with WHR increases when the target of hydrogen is increased. For the three scenarios respectively, a VALCOH decrease of 5.5%, 6.0% and 6.6% is observed when adding WHR to the system.

In the case were the PV ratio is not kept constant, the system behaves as a power plant when the objective of produced hydrogen is decreased and thus the VALCOH drops drastically. As this is out of the scope of this thesis, it is not looked into in more detail, but it gives rise to the conclusion that it is important to take into account the available space for PV panels at the chosen site when defining the objective of produced hydrogen.

Heating demand

In the waste heat recovery model, one of the key assumptions is the fact that the district heating networks at both temperature levels are infinite heat sinks, meaning that there are no limitations to the heating power that can be delivered to the DHNs. This assumption is adjusted in the following section of the sensitivity analysis. Two scenarios are investigated: the case where no heat exchange to a high-temperature DHN is possible, reffered to as MT Scenario, and the case where a certain heating demand pro-

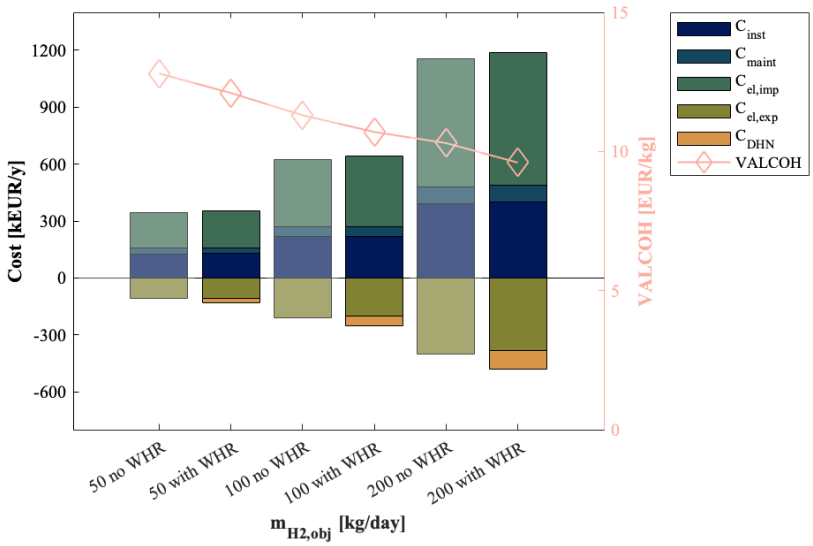

Figure 4.8: Summary of costs for the scenarios with different targets of produced hydrogen with and without the implementation of WHR; weight of cost categories on the left-hand axis and the VALCOH on the right-hand axis.

file is required to be met, referred to as 4xNEST. The influence of these limitations on VALCOH, equipment sizing and site operation are looked into.

First of all, the MT Scenario is investigated. Table 4.6 shows the selected size of the electrolyser, heat pump and heat exchanger for both the baseline and current scenario. As there is no heat delivered to the DHN at high temperature, no heat pump is selected for this configuration, but a heat exchanger is.

Summarized in Figure 4.9 are the VALCOH and large cost groups for the baseline scenario, the MT Scenario and 4xNEST. The value-adjusted levelized cost of hydrogen is higher with the current layout than the baseline, but is still 4% lower than the system without waste heat recovery. This indicates that even without the availability of a HT DHN, it is still worthwhile to recover waste heat and export it to a MT DHN. Furthermore, the installation costs for the current scenario are lower than the baseline, as the decrease in cost due to the omission of a heat pump is larger than the slight increase due to electrolyser size. Maintenance costs are similar but slightly larger for the currently investigated scenario. The reason is the large cost associated with compressor maintenance. As the electrolyser and compressor sizes are closely tied together, an increase in electrolyser size means an increase in compressor size. The fact that the compressor maintenance is calculated as a fraction of the total (not the annualized) investment cost and the large value for this fraction (8%) causes an increase in maintenance costs even though investment costs are lower. As for the operational costs, they are also increased for the current scenario with respect to the baseline as detailed in Figure 4.9. It demonstrates that the increase in operational costs is mainly due to a decrease in revenues from

Table 4.6: Optimization results for the main sizing decision variables for the baseline and first scenario.

	S_e [kW]	S_{HP} [kW]	S_{HEX} [m^2]
Baseline	411	103	0
MT Scenario	421	0	1.9

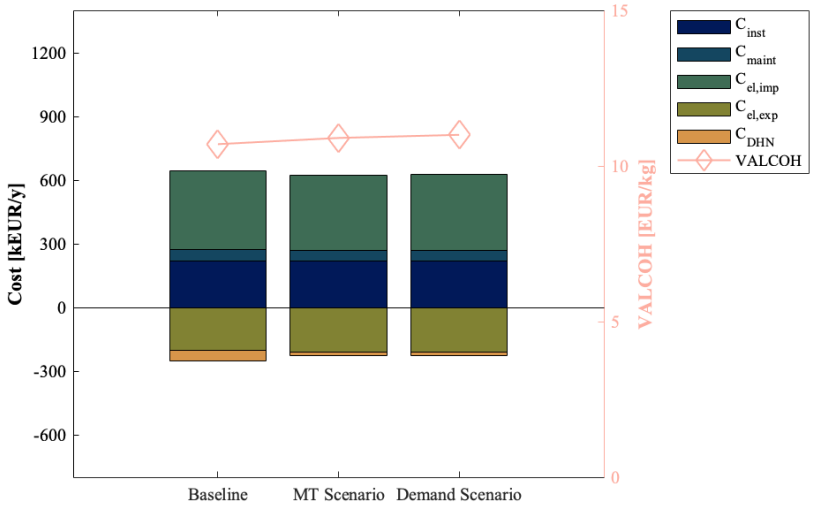

Figure 4.9: Summary of costs for the scenarios with different heating demand; weight of cost categories on the left-hand axis and the VALCOH on the right-hand axis.

the district heating network as high-temperature heat is more profitable than medium-temperature heat. A smaller influence is attributed to a decrease in imported electricity, as the electrical requirements of the heat pump no longer need to be met and the heat exchanger delivers heat to the MT DHN without requiring electricity. Thus, 3% more of the PV-generated electricity can be exported to the grid.

Another aspect of the current scenario is the heat recovery profile, shown in Figure 4.10 for a single week in every season of the year. In this system, where heat can only be delivered to the MT DHN, all recovered heat is delivered to the DHN as long as it generates revenues. The revenues are calculated as a specific fraction of the electricity prices, as shown in Table 3.1. In summer, this multiplying factor is negative for delivery to the MT DHN, meaning that a cost is incurred when heat is delivered during that time of year. Since this is not desirable, the heat is dissipated to the ambient using the dry cooler in summer, as seen in Figure 4.10c. At every other time of the year, all the electrolyser heat that is not lost due to system inefficiencies will be exported to the DHN at medium temperature.

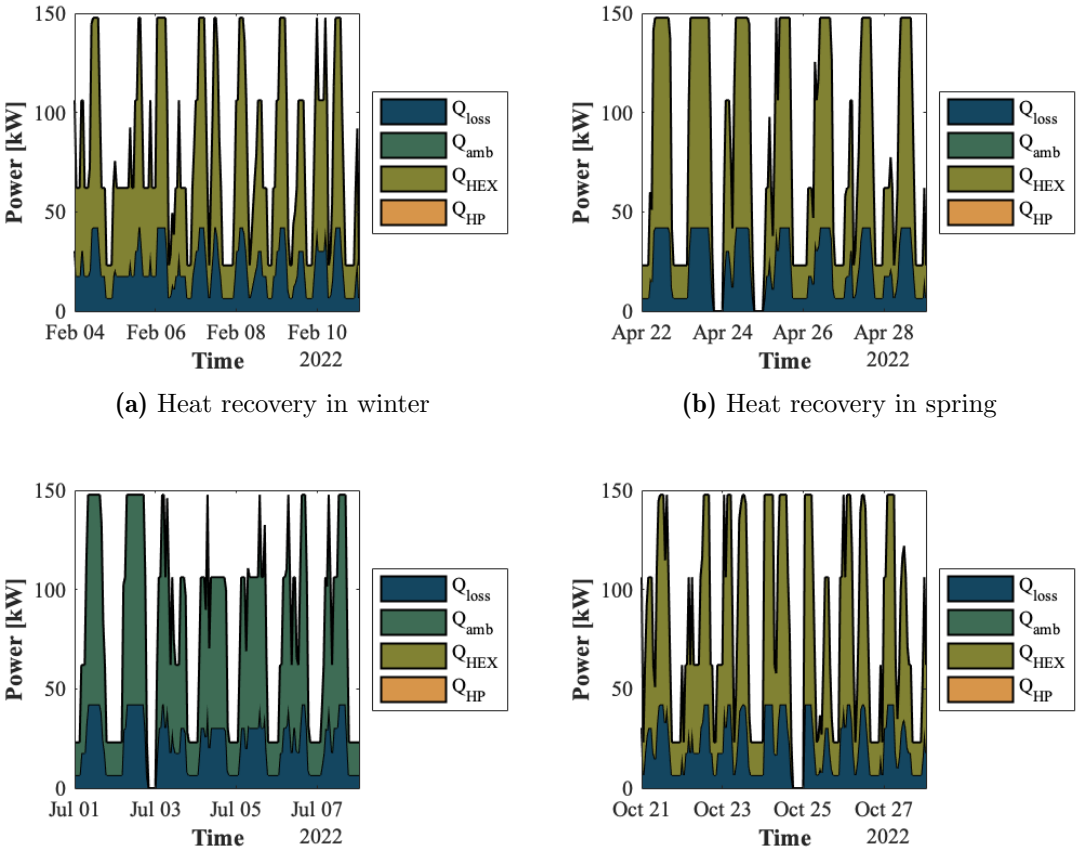

(a) Heat recovery in winter

(b) Heat recovery in spring

(c) Heat recovery in summer

(d) Heat recovery in autumn

Figure 4.10: Waste heat recovery profile when no heat can be delivered to the high-temperature DHN for four representative weeks, one in every season of the year.

The second scenario that is investigated in this paragraph is 4xNEST scenario. Here, the heat delivered to both district heating networks cannot exceed a demand profile. The chosen profile is the known demand for the NEST building at Empa throughout 2022, whose characteristics are shown in Table 4.7 [4]. As this demand reflects the demand of just a single building, a multiple of the profile is used as an upper boundary to the exported heat, calculated as follows. If the electrolyser runs year-round at 50% of the nominal power, the total amount of heat generated by the electrolyser is equal to 653 MWh, which corresponds to the heat demand of 5.1 NEST buildings. Further, a margin is taken into account to correct for heat losses in the system. Thus, conservatively, it is assumed that 4 buildings can be provided with heat from the hydrogen generation site and the demand is 4 times that of NEST.

Table 4.8 summarizes the size and choice of equipment for this scenario and the baseline. As the demand profile includes heat that is exchanged to both the high- and medium-temperature DHN, both a heat pump and heat exchanger are selected. The size of the

Table 4.7: District heating network demand NEST building in 2022 [4].

	E_{tot} [MWh/y]	$P_{peak,HT}$ [kW]	$P_{avg,HT}$ [kW]	$P_{peak,MT}$ [kW]	$P_{avg,MT}$ [kW]
NEST demand	127.5	18.0	1.6	61.0	13.0 height

Table 4.8: Optimization results for the main sizing decision variables for the baseline and 4xNEST Scenario.

	S_e [kW]	S_{HP} [kW]	S_{HEX} [m^2]
Baseline	411	103	0
4xNEST Scenario	418	12	1.8

heat pump is significantly smaller than in the baseline scenario, as the demand for high temperature heat is lower.

Figure 4.9 demonstrates the value-adjusted levelized cost of hydrogen increases in this alternative operation, this time with 3%, which makes the value slightly higher than the case where heat can only be exported to the MT DHN. As was valid for the MT Scenario, the yearly investment costs are lower in the 4xNEST Scenario due to a smaller heat pump, despite the presence of a larger electrolyser. Similarly, the maintenance costs have also increased slightly with the compressor size. The biggest difference with the baseline can be seen in the operational costs, which increase by 11%. The highest contributor to this increase is once more the decrease in revenues from the district heating network. The amount of imported electricity has decreased due to the decrease in heat pump size, which also results in a slightly higher amount of exported electricity.

The profile for waste heat recovery for this scenario is found in Figure 4.11 for four weeks throughout the year. During every season, the required heat is delivered to the high-temperature DHN, whereas for the medium-temperature DHN, the demand is satisfied in winter, spring and autumn. In summer, the system chooses not to deliver any heat as it would incur costs.

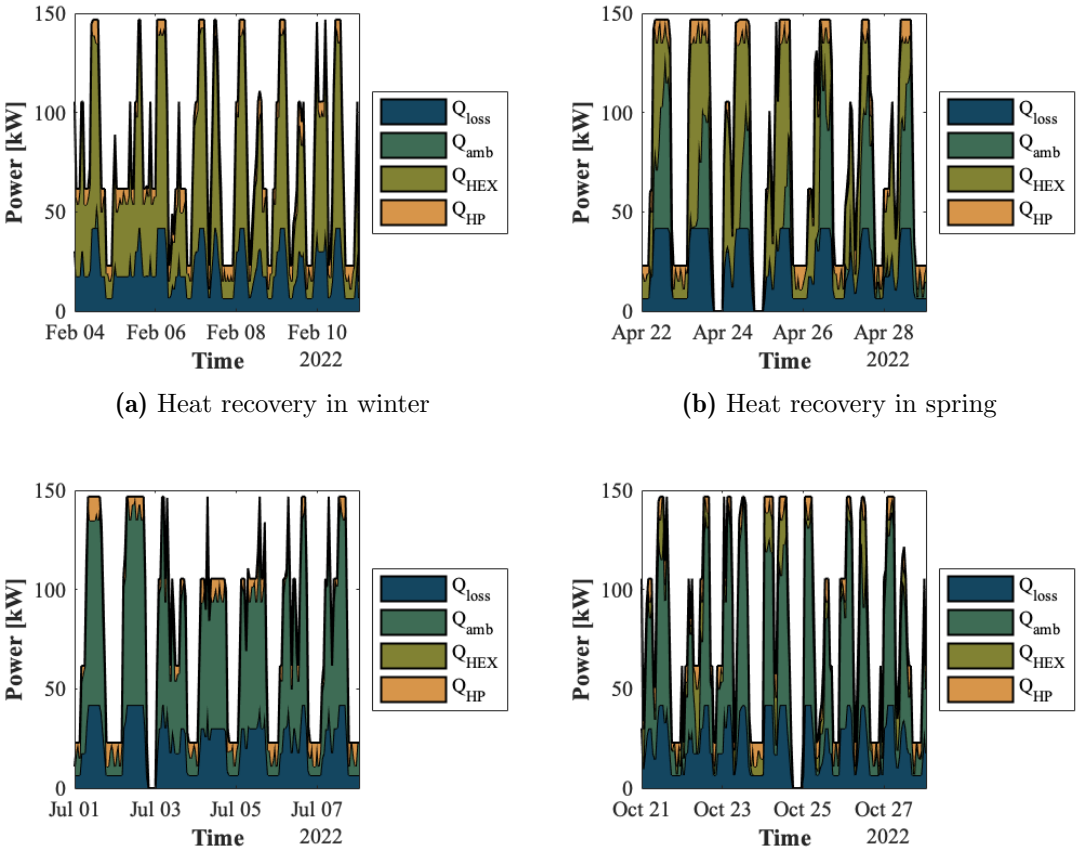

(a) Heat recovery in winter

(b) Heat recovery in spring

(c) Heat recovery in summer

(d) Heat recovery in autumn

Figure 4.11: Waste heat recovery profile when the 4xNEST demand profile is matched for four representative weeks, one in every season of the year.

A full comparison of the heat recovery in every season for the three discussed WHR scenarios is shown in Figure 4.12. As already explained, no heat is exchanged in summer when only the MT DHN is available. Moreover, although there is no limitation to the amount of heat that can be delivered to the MT DHN, the absolute amount of heat recovered in every season is slightly lower than for the baseline scenario. This can be attributed to slightly different electrolyser sizes and operation throughout the year. Thus the total fraction of heat recovery in this scenario is 0.53, 25.3% lower than the baseline scenario. When the multiple of the NEST heating demand profile is followed, a WHR fraction of 0.36 is found, 49.2% lower than baseline. This can be attributed to a mismatch in electrolyser operation and heating demand, namely that the moments when it is cheapest to run the electrolyser do not coincide with the moments of greatest heat demand. As the export cost of heat is only a small fraction of the import cost of electricity, electrolyser operation will follow the former trend more than the latter. Furthermore, the WHR fraction could be increased in the 4xNEST scenario by increasing

the number of buildings the hydrogen generation site can supply heat to. However, it might be relevant to then take into account the cost of heat not supplied, in seasons other than summer and for the MT DHN (because heat export in this case will not take place as long as it generates costs).

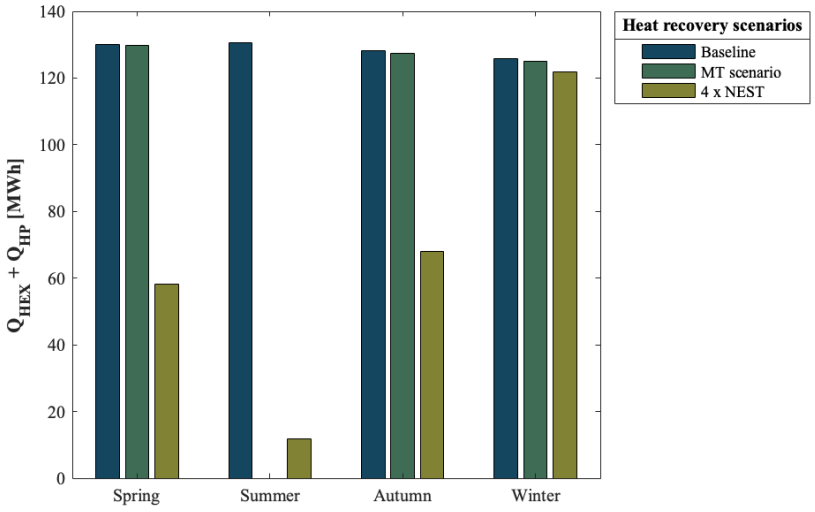

Figure 4.12: The total amount of recovered heat in every season per heat recovery scenario.

Chapter 5

Conclusions and Outlook

5.1 Conclusions

In this work, a model for the optimal sizing and operation of a hydrogen generation site was expanded. This model incorporated continuous sizing of all major components, piecewise affine (PWA) approximations of components' efficiency, and the recovery of waste heat from the electrolyser to a medium- or high-temperature district heating network. The system model was formulated as a MILP problem in MATLAB and solved using the Gurobi optimizer. The thermal model was verified by comparing heat recovery fractions with experimental data from the electrolyser at MOVE, in Dübendorf, Switzerland. Further, the model was applied to a hypothetical case study also in Dübendorf, Switzerland, for the year 2022.

The first research question addressed in this work pertained to the optimal size and operation of components in a hydrogen generation site with waste heat recovery (WHR), with the aim to minimize total cost. It was found that when the system is optimized for both the sizing and operation of the site components simultaneously, and waste heat recovery is included, the value-adjusted levelized cost of hydrogen (VALCOH) was 18.9% lower than the scenario without WHR, with sizing methods from a reference paper.

Secondly, the influence of the level of fidelity of the modelling on the optimal solution was investigated. In this context, the electrolyser was found to operate more at partial load when the efficiency curve was considered, resulting in operation at higher efficiency. Additionally, the optimal component size increased with increasing accuracy of the PWA approximation, allowing for more operational flexibility within the selected nominal power to operate at part load. This higher initial investment cost allowed a decrease in operational cost. Thus, increasing the accuracy of the electrolyser operation from a constant efficiency to a PWA approximation with four breakpoints decreased the VALCOH by 3.9%.

Furthermore, for a system optimized for minimal cost, the heat recovery system consid-

ered heat exports only to the high-temperature district heating network. Consequently, a heat pump was installed and no heat exchanger was included.

Lastly, the parameters with the largest influence on the objective function were identified. Upon inspecting the global sensitivity of the model, the electrolyser efficiency and electricity prices were shown to have a significant influence on the objective function. Moreover, an increase in efficiency greatly decreased the VALCOH and reduced the benefit of adding a heat recovery system. The sensitivity of the system regarding the target of produced hydrogen was also analyzed, and it was observed that higher production targets resulted in lower VALCOH and a higher benefit to adding WHR to the system. Additionally, multiple heat demand scenarios were examined, and considering a realistic heat demand profile altered the components selected for the heat recovery system to include a heat exchanger in addition to the heat pump.

In conclusion, this work demonstrated the importance of simultaneous optimization for size and operation of components, as well as the relevance of adding WHR to lower costs of the hydrogen generation site. In addition, it was found that an accurate representation of the electrolyser efficiency aids in decreasing the VALCOH of the system. As a matter of consequence, it is important to consider and model these factors in the design of new hydrogen generation sites moving forward.

5.2 Outlook

In order to build on the research done in this thesis, several concepts can be looked at or worked out in more detail. Some possible directions of research to explore are set out below:

- In Section 3.2 the heat recovery system is verified against data from MOVE, but a thorough validation of the heat recovery system is still to be done.
- In this work, efficiency is deemed the same for electrolysers regardless of their size. However, the efficiency curve is affected by the device size, therefore it would be interesting to look into the use of size-efficiency correlations in future works.
- The battery is not yet selected in the system due to its high cost, but when the cost of battery is low enough to be included, it is possible to implement its efficiency curve while charging and discharging.
- Extension of the model to include different waste streams from the electrolyser, such as oxygen [43], can be done.
- Investigation of the feasibility of electrolyser operation at high temperature can be interesting, such that passive heat exchange to a high-temperature DHN is possible with a heat exchanger instead of a heat pump.
- Better modelling of the electrolyser start-up and degradation over time can be done by including data from a running electrolyser.

- Investigation of the benefits of recovering heat from other components in the hydrogen generation plant such as the compressor, or a fuel cell (where it is implemented) is of interest as well.

Appendices

Appendix A

Battery efficiency

The efficiency of the battery depends on the rate of (dis)charge, or C-rate of the battery. This is defined as follows:

$$C{-}rate = \frac{SOC(t) - SOC(t-1)}{\Delta t}\, 3600 \tag{A.1}$$

Since the state of charge of the battery is not (directly) a decision variable of this problem, this equation is rewritten by using equations 2.27 and **??** to come to the following definition:

$$C{-}rate = \frac{P_{b,ch} - P_{b,disch}}{C_b}\, 3600 \tag{A.2}$$

A linearization of the battery efficiency would result in an equation of the following format:

$$\eta_b = m * C{-}rate + q \tag{A.3}$$

The main problem with the non-linearity results from Equation 2.23, where the following term is present after rearrangement:

$$\frac{P_{b,ch}}{\eta_b} - P_{b,disch}\, \eta_b \tag{A.4}$$

Here, the charging and discharging power are divided and multiplied by the battery efficiency respectively. Inserting the definition of the efficiency and substituting the C-rate, equation A.4 becomes:

$$\frac{P_{b,ch}}{m\, \frac{P_{b,ch} - P_{b,disch}}{C_b}\, 3600 + q} - P_{b,disch} \left(m\, \frac{P_{b,ch} - P_{b,disch}}{C_b}\, 3600 + q \right) \tag{A.5}$$

Substituting $P_{b,ch}$ for x, $P_{b,disch}$ for y, C_b for C and $m * 3600$ for m', to alleviate the notation, and further trying to simplify the equation, the following is found:

$$\frac{x\, C - (m')^2 \left[x^2\, y/C + y^3/C - 2x\, y^2/C \right] - 2\, m'\, q\, (xy - y^2) - q^2\, y\, C}{m'\, (x - y) + q\, C} \tag{A.6}$$

As the equation shows, this is not a simplification in the least. It does demonstrate, however, the complexity of the issue and its non-linearity. Due to this, the ambition to include a piecewise affine approximation of the battery efficiency is dropped.

[2]

Appendix B

Cost data

Table B.1: Cost data for all components.

	UP_i	l_i [y]	μ_i	References
PV	800	30	0.0158	[16], [2]
Battery	600	10	0.02	[16], [1]
Electrolyser	-	7	0.02	[2], [16]
Heat Pump	576	20	0.015	[30], [1]
Heat Exchanger*	77.79	20	0.015	[21]
Compressor	-	10	0.08	[2]
H_2 Storage	1644	10	0.03	[2]
Refrigerator	5374	15	0.03	[2]
H_2 Dispenser	65 000	10	0.03	[2]

*Note for heat exchanger: fixed cost of 5292 EUR is added in the scenarios where a heat exchanger is chosen.

Table B.2: Remaining techno-economic data.

	Used value
$\eta_{ref,PV}$	0.15
η_b	0.92
d	0.04
$P_{PV,max}$	1500 kW
Operating T PEM	70 °C
c_p	4.186 kJ/(kg K)
HHV H_2	39.39 kWh/kg
COP_{real}	8.25

Appendix C

Input data 2018

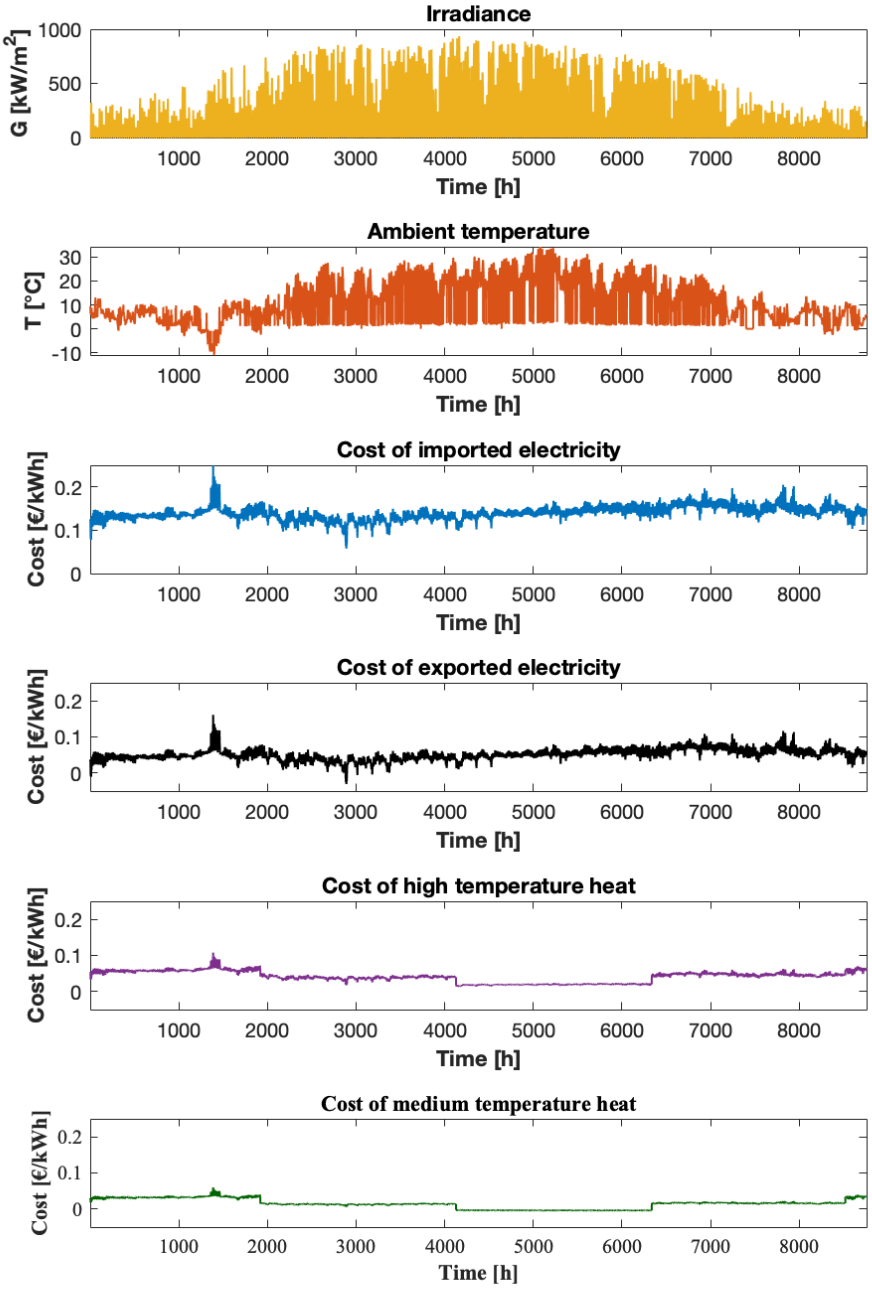

Figure C.1: Summary of input data for the year 2018.

Bibliography

[1] P. Gabrielli, M. Gazzani, E. Martelli, and M. Mazzotti, "Optimal design of multi-energy systems with seasonal storage," *Applied Energy*, vol. 219, pp. 408–424, 6 2018.

[2] M. Minutillo, A. Perna, A. Forcina, S. D. Micco, and E. Jannelli, "Analyzing the levelized cost of hydrogen in refueling stations with on-site hydrogen production via water electrolysis in the italian scenario," *International Journal of Hydrogen Energy*, vol. 46, pp. 13667–13677, 4 2021.

[3] G. Humbert, H. Cai, B. P. Koirala, and P. Heer, "Cost-effective hydrogen generation: Concurrent optimization of component sizes and system operation."

[4] Empa, "Nest wiki." `https://info.nestcollaboration.ch/wikipediapublic`. [Online; accessed: 15.09.2023; data from 01/01/2022-31/12/2022].

[5] E. Council, "Fit for 55." `https://www.consilium.europa.eu/en/policies/green-deal/fit-for-55-the-eu-plan-for-a-green-transition/`, 2023. [Online; accessed: 12.12.2023].

[6] D. J. Jovan and G. Dolanc, "Can green hydrogen production be economically viable under current market conditions," *Energies*, vol. 13, 12 2020.

[7] S. Sagaria, A. Moreira, F. Margarido, and P. Baptista, "From microcars to heavy-duty vehicles: Vehicle performance comparison of battery and fuel cell electric vehicles," *Vehicles*, vol. 3, pp. 691–720, 12 2021.

[8] IEA, "The future of hydrogen," 2019.

[9] E. Commission, "Powering a climate-neutral economy: An eu strategy for energy system integration," 2020.

[10] V. Andiappan, Y. K. Wan, and D. K. S. Ng, "Process systems engineering for decarbonisation strategies and systems," *Process Integration and Optimization for Sustainability*, vol. 5, pp. 173–174, 2021.

[11] V. Vahidinasab and B. Mohammadi-Ivatloo, *Energy Systems Transition - Digitalization, Decarbonization, Decentralization and Democratization.* Springer, 2023.

[12] F. Jonsson and A. Miljanovic, "Utilization of waste heat from hydrogen production a case study on the botnia link h2 project in lulea, sweden," 2022.

[13] A. Perna, M. Minutillo, S. D. Micco, and E. Jannelli, "Design and costs analysis of hydrogen refuelling stations based on different hydrogen sources and plant configurations," *Energies*, vol. 15, 1 2022.

[14] W. J. Tiktak, "Heat management of pem electrolysis."

[15] A. H. Reksten, M. S. Thomassen, S. MÃ¸ller-Holst, and K. Sundseth, "Projecting the future cost of pem and alkaline water electrolysers; a capex model including electrolyser plant size and technology development," *International Journal of Hydrogen Energy*, vol. 47, pp. 38106–38113, 11 2022.

[16] A. Ibanez-Rioja, P. Puranen, L. Jarvinen, A. Kosonen, V. Ruuskanen, J. Ahola, and J. Koponen, "Simulation methodology for an off-grid solarâbatteryâwater electrolyzer plant: Simultaneous optimization of component capacities and system control," *Applied Energy*, vol. 307, 2 2022.

[17] I. Sorrenti, T. B. Rasmussen, G. Xydis, P. Enevoldsen, and S. You, "Correlations between component size green hydrogen demand and breakeven price for energy islands," *Renewable and Sustainable Energy Reviews*, vol. 183, p. 113439, 9 2023.

[18] M. T. Baumhof, E. Raheli, A. G. Johnsen, and J. Kazempour, "Optimization of hybrid power plants: When is a detailed electrolyzer model necessary?," Institute of Electrical and Electronics Engineers Inc., 2023.

[19] P. Gabrielli, B. Flamm, A. Eichler, M. Gazzani, J. Lygeros, and M. Mazzotti, *Modeling for Optimal Operation of PEM Fuel Cells and Electrolyzers*. IEEE, 2016.

[20] P. Marocco, D. Ferrero, E. Martelli, M. Santarelli, and A. Lanzini, "An milp approach for the optimal design of renewable battery-hydrogen energy systems for off-grid insular communities," *Energy Conversion and Management*, vol. 245, 10 2021.

[21] E. van der Roest, R. Bol, T. Fens, and A. van Wijk, "Utilisation of waste heat from pem electrolysers - unlocking local optimisation," *International Journal of Hydrogen Energy*, 2023.

[22] Empa, "Move - virtual." `https://move.nestcloud.ch`. [Online; accessed: 12.12.2023].

[23] G. Sansavini, "Optimal design of multi-energy systems (mes) and technology modelling." ETH Zurich, 2021. [PowerPoint Slides].

[24] S. Dubey, J. N. Sarvaiya, and B. Seshadri, "Temperature dependent photovoltaic (pv) efficiency and its effect on pv production in the world - a review," vol. 33, pp. 311–321, Elsevier Ltd, 2013.

[25] W. D. Soto, S. A. Klein, and W. A. Beckman, "Improvement and validation of a model for photovoltaic array performance," *Solar Energy*, vol. 80, pp. 78–88, 2006.

[26] V. Sun, A. Asanakham, T. Deethayat, and T. Kiatsiriroat, "A new method for evaluating nominal operating cell temperature (noct) of unglazed photovoltaic thermal module," *Energy Reports*, vol. 6, pp. 1029–1042, 11 2020.

[27] C. Huang, Y. Zong, S. You, and C. TrÃ¦holt, "Economic model predictive control for multi-energy system considering hydrogen-thermal-electric dynamics and waste heat recovery of mw-level alkaline electrolyzer," *Energy Conversion and Management*, vol. 265, 8 2022.

[28] J. J. C. Mancera, F. S. Manzano, J. M. Andujar, F. J. Vivas, and A. J. Calderon, "An optimized balance of plant for a medium-size pem electrolyzer. design, control and physical implementation," *Electronics (Switzerland)*, vol. 9, 5 2020.

[29] T. Laaksonlaita, "Modelling, identification and control of a renewable hydrogen production system for mobility application,"

[30] M. Fiorentini, P. Heer, and L. Baldini, "Design optimization of a district heating and cooling system with a borehole seasonal thermal energy storage," *Energy*, vol. 262, 1 2023.

[31] R. Hackl and S. Harvey, "Identification, cost estimation and economic performance of common heat recovery systems for the chemical cluster in stenungsund project report," 2013.

[32] A. H. Hermelink, D. D. Jager, K. Jensen, and S. Norway, "The crucial role of discount rates in european commission energy system modelling," 2015.

[33] Agora-Industry, "Levelised cost of hydrogen: Making the application of the lcoh concept more consistent and more useful." `www.agora-industry.org`, July 2023.

[34] M. Balesdent, L. Brevaul, S. Lacaze, S. Missoum, and J. Morio, *Methods for high-dimensional and computationally intensive models*, pp. 109–136. Elsevier Inc., 2016.

[35] A. A. Saltelli, *Global sensitivity analysis : the primer*. John Wiley, 2008.

[36] . Mr (2023). Sensitivity Analysis Morris method (advanced) (https://www.mathworks.com/matlabcentral/fileexchange/48884-sensitivity-analysis-morris-method advanced), MATLAB Central File Exchange. Retrieved October 6

[37] L. Xia, Z. Ma, G. Kokogiannakis, Z. Wang, and S. Wang, "A model-based design optimization strategy for ground source heat pump systems with integrated photovoltaic thermal collectors," *Applied Energy*, vol. 214, pp. 178–190, 3 2018.

[38] N. P. of Worldwide Energy Resources, "The power project." `https://power.larc.nasa.gov`. [Online; accessed: 20.6.2023].

[39] ENTSO-E, "Transparency platform - day ahead prices." `https://transparency.entsoe.eu/dashboard/show?loggedUserIsPrivileged=false`. [Online; accessed: 20.6.2023].

[40] L. Baldini, *Dynamic Energy Weighting Factors to Promote the Integration of Renewables into Buildings*. Sustainable Built Environment (SBE) Regional Conference Zurich, 2016.

[41] Empa, "Nest wiki." `https://info.nestcollaboration.ch/wikipediapublic`. [Online; accessed: 24.10.2023; data from 16/08/2023-22/10/2023].

[42] M. N. I. Salehmin, T. Husaini, J. Goh, and A. B. Sulong, "High-pressure pem water electrolyser: A review on challenges and mitigation strategies towards green and low-cost hydrogen production," 9 2022.

[43] G. Maggio, G. Squadrito, and A. Nicita, "Hydrogen and medical oxygen by renewable energy based electrolysis: A green and economically viable route," *Applied Energy*, vol. 306, 1 2022.